2003

Cronin effect and high-pT suppression in pA collisions

Dmitri Kharzeev, *Brookhaven National Laboratory*
Yuri V. Kovchegov, *University of Washington - Seattle Campus*
Kirill Tuchin, *University of Washington - Seattle Campus*

Cronin effect and high-p_T suppression in pA collisions

Dmitri Kharzeev
Nuclear Theory Group, Brookhaven National Laboratory, Building 510A, Upton, New York 11973, USA

Yuri V. Kovchegov
Department of Physics, University of Washington, Box 351560, Seattle, Washington 98195, USA

Kirill Tuchin
Institute for Nuclear Theory, University of Washington, Box 351550, Seattle, Washington 98195, USA

(Received 3 July 2003; published 18 November 2003)

We review the predictions of the theory of a color glass condensate for a gluon production cross section in $p(d)A$ collisions. We demonstrate that, at moderate energies, when the gluon production cross section can be calculated in the framework of the McLerran-Venugopalan model, it has only a partonic level Cronin effect in it. At higher energies or rapidities corresponding to smaller values of the Bjorken x, quantum evolution becomes important. The effect of quantum evolution at higher energies or rapidities is to introduce the suppression of high-p_T gluons slightly decreasing the Cronin enhancement. At still higher energies or rapidities quantum evolution leads to the suppression of produced gluons at all values of p_T.

DOI: 10.1103/PhysRevD.68.094013 PACS number(s): 13.85.Hd, 13.60.Hb, 13.85.Ni

I. INTRODUCTION

Recently there has been a surge of interest in particle production in proton-nucleus (pA) and deuteron-nucleus (dA) collisions at high energies. The interest was inspired by the new data produced by the dA program at the BNL Relativistic Heavy Ion Collider (RHIC) [1–4], which should enable one to separate the contributions of the initial state effects [8] such as parton saturation [9–13] from the final state effects, such as jet quenching and energy loss in the quark-gluon plasma (QGP) [14–17], to the suppression of high transverse momentum particles observed in Au-Au collisions at RHIC [5–7].

Saturation physics has been largely successful in describing hadron multiplicities in Au-Au collisions at RHIC [18]. It can also have important implications for the transverse momentum distributions [19], particle correlations, and azimuthal anisotropies [20]. It has been demonstrated [21] that saturation provides very favorable initial conditions for the thermalization of parton modes with the transverse momenta $k_T \sim Q_s$, where Q_s is the saturation scale. The thermalization was also found [21] to approximately preserve the centrality dependence of total hadron multiplicities determined by the initial conditions [18]. Recent lattice results [22,23] show that the initial average transverse momentum $\langle k_T \rangle$ of the produced partons is $\langle k_T \rangle \sim Q_s$, which makes the ''soft thermalization'' scenario preserving the initial centrality and rapidity distributions quite likely. Final state interactions, however, will undoubtedly modify the transverse momentum distributions at $k_T \leqslant (1-3) Q_s$ without introducing a new momentum scale [21]. If the produced medium lives long enough, then high k_T jets will be suppressed as well because of the jet quenching and energy loss [14–17].

The first d-Au data from RHIC show a Cronin enhancement extending up to $k_T \simeq 6$ GeV around $y \sim 0$ [1,3] whereas at slightly forward rapidity around $y \sim 1$ no significant enhancement is seen [2]. The absence of suppression indicates that final state interactions are indeed responsible for the effect observed in Au-Au collisions [5–7] in the same k_T range. However, the nonuniversality of the ratios for the charged hadron and π^0 spectra [1] indicate deviations from the independent jet fragmentation up to $k_T \simeq 5$ GeV. Similar nonuniversality in the same k_T range was observed for Λ and K production [24], and in $p, \bar{p}$ and pion production [25] in Au-Au collisions. It remains to be checked if there is a statistically significant suppression of high k_T charged hadron and π^0 yields above the Cronin enhancement region ($k_T \geqslant 6$ GeV), and if this suppression depends on centrality of d-Au collisions. This question is of crucial importance for the interpretation of the spectacular effect observed in Au-Au collisions [5–7] because this is the kinematical region in which the independent jet fragmentation picture, and thus the perturbative jet quenching description, begin to apply.

The first dA data from RHIC [1–3] give the ratio of the number of particles produced in a dA collision over the number of particles produced in a pp collision scaled by the number of collisions

$$R^{dA}(k_T, y) = \frac{\dfrac{dN^{dA}}{d^2k dy}}{N_{\rm coll} \dfrac{dN^{pp}}{d^2k dy}}. \tag{1}$$

To understand the new data on R^{dA} and what it implies for our understanding of high energy nuclear wave functions we are going to study here the expectations for R^{dA} from saturation physics. Our approach will be somewhat academic: in this paper, we will not include explicitly all of the effects related to the fact that high-k_T of produced particles corresponds to a rather large Bjorken x in the actual RHIC experiments at central rapidity—the effective Bjorken x of high-k_T ($k_T > 5$ GeV) particles observed at midrapidity at RHIC at

$\sqrt{s}=200$ GeV is about $x\approx 0.1$ which may be too large for the small-x treatment that we present here (see [26], but see also [27]). These finite-energy effects have to be accurately accounted for before we can compare our calculations to the data. Nevertheless, we feel that a better understanding of the qualitative features of hadron production within the saturation framework is a necessary prerequisite for a complete theoretical description of high energy $p(d)$-A collisions.

We assume that collisions take place at very high energy such that the effective Bjorken x is sufficiently small for all k_T of interest. For simplicity we will analyze proton-nucleus collisions assuming that the main qualitative conclusions would be applicable to dA. Since we cannot calculate $N_{\rm coll}$ in a model-independent way, we will be using Eq. (32) for our definition of R^{pA}, which is identical to Eq. (1) applied to pA collisions with a proper definition of $N_{\rm coll}$ (see [28] for a discussion of uncertainties involved in theoretical evaluations of this quantity).

The problem of gluon production in pA collisions has been solved in the framework of the McLerran-Venugopalan model [12] in [29] (see also [30–33]). The resulting cross section includes the effects of all multiple rescatterings of the produced gluon and the proton in the target nucleus [29]. At higher energy quantum evolution becomes important [34–41]. In the large N_c limit the small-x evolution equation can be written in a nonlinear integro-differential form [35–38] shown here in Eq. (49). The inclusion of nonlinear evolution [35–38] in the quasi-classical gluon production cross section of [29] has been done in [42] (see also [43,44]). The study of the resulting gluon spectrum and corresponding gluonic R^{pA} is the goal of this paper.

The paper is organized as follows. In Sec. II A we discuss two main definitions of unintegrated gluon distribution functions: the standard definition (2) and the one inspired by the non-Abelian Weizsäcker-Williams field of a nucleus in the McLerran-Venugopalan model (6) [12,13]. We argue, following [42,45], that Eq. (6) is the correct definition of the unintegrated gluon distribution counting the number of gluon quanta. We proceed by analyzing k_T dependence of the distribution functions. In Sec. II B we prove the sum rules for both distribution functions given in Eqs. (12) and (13), which are valid in the quasi-classical approximation only. In the framework of the McLerran-Venugopalan model [12,46] the sum rules insure that the presence of shadowing in nuclear gluon distribution functions in the saturation regime ($k_T \lesssim Q_{s0}$) requires enhancement of gluons at higher k_T($k_T \gtrsim Q_{s0}$) reminiscent of antishadowing. This conclusion is quantified in Sec. II C [see Fig. 3 and Eqs. (28) and (29)] and the differences between distribution functions are clarified [see Eqs. (23) and (24)]. However, as we demonstrate in Sec. II B, the sum rules break down once quantum evolution with energy [35–38] is included. They turn into inequalities (19) and (20). This indicates that, while multiple rescatterings in the McLerran-Venugopalan model only redistribute gluons in transverse momentum phase space conserving the total number of gluons in the nucleus [29], quantum evolution of [35–38] actually reduces the number of gluons in the nuclear wave functions at a given value of the Bjorken x.

In Sec. III we study the gluon production cross section in pA in the quasi-classical approximation [29]. In Sec. III A we show that the gluon production cross section calculated in [29] in the McLerran-Venugopalan multiple rescattering model exhibits only Cronin-like enhancement [47], as shown in Fig. 4 and in Eq. (37) (cf. [48,49]). In the corresponding moderately high energy regime the height and k_T-position of the Cronin peak are increasing functions of centrality as can be seen from Eq. (38). In Sec. III B following [42] we point out that, surprisingly, the gluon production cross section in pA can be written in a k_T-factorized form (43) [9,50] with the unintegrated distribution functions defined by Eq. (2), the physical meaning of which is less clear than that of Weizsäcker-Williams ones (6). In Sec. III B we also prove a sum rule (46) which insures that suppression of produced gluons at low k_T($k_T \lesssim Q_{s0}$) demands Cronin-like enhancement at high k_T($k_T \gtrsim Q_{s0}$) in the McLerran-Venugopalan model. The relative amounts of suppression and enhancement are different from the quasi-classical gluon distribution case of Sec. II.

Multiple rescatterings of partons inside the nucleus are believed to be the cause of the Cronin effect. Phenomenologically these multiple rescatterings are usually modeled by introducing transverse momentum broadening in the nuclear structure functions [51–54]. In Sec. III we demonstrate how an explicit PQCD calculation of these multiple rescatterings done in [29] yields us the Cronin effect (cf. [48,49]).

Section IV is devoted to studying the effects of nonlinear evolution (49) on the gluon production cross section in pA. In Sec. IV A we use the analogy to the case of gluon production in deep inelastic scattering (DIS) solved in [42,44] to include the effects of evolution (49) in the gluon production cross section in pA. The result is given by Eq. (53). By expanding the all-twist formula (53) we then study the effect of nonlinear evolution on the gluon production at the leading twist (Sec. IV B) and next-to-leading twist (Sec. IV C) level. In Sec. IV B we start by deriving gluon production cross section at the leading twist level (62). We then estimate the cross section for high k_T[$k_T > k_{\rm geom} \gg Q_s(y)$] in the double logarithmic approximation (66) [50] and demonstrate that the corresponding R^{pA} is approaching 1 at high k_T from below, i.e., that $R^{pA}<1$ at $k_T \gg Q_s(y)$ [see Eq. (75)]. We proceed by evaluating Eq. (62) in the extended geometric scaling region [$Q_s(y) < k_T \lesssim k_{\rm geom}$] [45,55,56]. The resulting leading twist gluon production cross section (86) leads to further suppression of gluon production due to the change in gluon anomalous dimension [8] as shown in Eqs. (89) and (91). At very high energies when the gluon production in pp is also in the extended geometric scaling region ($k_T < k_{\rm geom}^p$) the ratio R^{pA} saturates at $R^{pA}\sim A^{-1/6}$, as follows from Eq. (92). The next-to-leading twist contribution to the gluon production cross section in pA is evaluated in Sec. IV C with the result given by Eqs. (98) and (99). One can see that the subleading twist term contributes towards enhancement of gluon production at high k_T. However, in the k_T region where the next-to-leading twist contribution dominates over higher twists it is small compared to the leading twist term. Therefore the positive sign of the higher twist term cannot alter our conclusion of high-k_T suppression we derived by analyzing leading twist. To understand how all twists add up we study what

happens to the Cronin peak [$k_T \sim Q_s(y)$] at high energy in Sec. IV D. We find that the height of the Cronin maximum decreases with energy and eventually the Cronin peak flattens out at the same level as the rest of R^{pA} at higher k_T, which is shown in Eq. (113). In Sec. IV E we observe that inclusion of evolution only strengthens the suppression of R^{pA} at low k_T[$k_T \ll Q_s(y)$] [see Eq. (116)] which was observed before in Sec. III B in the quasi-classical case. In Sec. IV F we construct a toy model illustrating the conclusion of Sec. IV that quantum evolution [35–38] introduces suppression of R^{pA} at all values of k_T (see Fig. 8). We demonstrate that quantum evolution not only suppresses R^{pA} making it less than 1, but also turns R^{pA} into a decreasing function of collision centrality contrary to the quasi-classical expectations.

We conclude in Sec. V by summarizing our results.

II. A TALE OF TWO GLUON DISTRIBUTION FUNCTIONS

A. Definitions

There are two different ways to define unintegrated gluon distribution function of a proton or nucleus. The most conventional way relates it to the $q\bar{q}$ dipole cross section on the target nucleus via two gluon exchange. Here we are going to use a similar definition relating the unintegrated gluon distribution to the dipole cross section on the nucleus (see Fig. 1).

The corresponding gluon distribution is given by (cf. [41,43])

$$\phi(x,\boldsymbol{k}^2)=\frac{C_F}{\alpha_s(2\pi)^3}\int d^2b\,d^2r\,e^{-i\boldsymbol{k}\cdot\boldsymbol{r}}\,\nabla_r^2 N_G(\boldsymbol{r},\boldsymbol{b},y=\ln 1/x), \tag{2}$$

where $N_G(\boldsymbol{r},\boldsymbol{b},y=\ln 1/x)$ is the forward amplitude of a gluon dipole of transverse size $\boldsymbol{r}$ at impact parameter $\boldsymbol{b}$ and rapidity y scattering on a nucleus [35,42]. We denote by $\boldsymbol{k}$ the transverse components of the four-vector k, and by k_T its length. The definition of Eq. (2) is inspired by k_T factorization and is valid as long as one can neglect multiple rescatterings of the dipole in the nucleus. By using Eq. (2) in the saturation region where higher twists (multiple rescatterings) become important one implicitly assumes that there exists a certain gauge in which the $q\bar{q}$ dipole cross section on a nucleus is given by a two gluon exchange interaction between the dipole and the nucleus and the interaction shown in Fig. 1 is literally all one needs to obtain the correct dipole cross section. It is not clear at present whether this is the case and such a gauge exists. Therefore the gluon distribution given by Eq. (2) does not give one the number of gluons in the nuclear wave function in the saturation region. The applications of the definition (2) will be clarified later.

Another definition of unintegrated gluon distribution literally counts the number of gluons in the nuclear wave function. To construct it in the quasi-classical limit of high energy QCD given by the McLerran-Venugopalan model [12] one has to first find the classical gluonic field of the nucleus in the light cone gauge of the ultrarelativistic nucleus (non-Abelian Weizsäcker-Williams field) and then calculate the correlator of two such fields to get the unintegrated gluon distribution function (see Fig. 2).

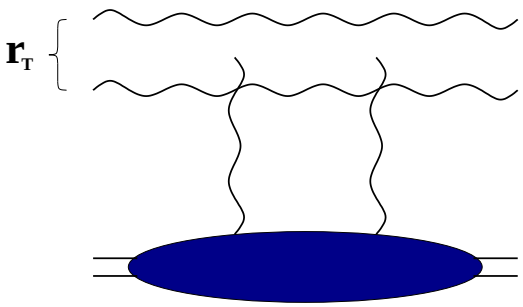

FIG. 1. "Conventional" definition of unintegrated gluon distribution relating it to the gluon dipole cross section. The exchanged gluon lines can connect to either gluon in the dipole.

The non-Abelian Weizsäcker-Williams field of a nucleus has been found in [13], leading to the following expression for the corresponding gluon distribution [13,29]:

$$\phi^{WW}(x,\boldsymbol{k}^2)=\frac{1}{2\pi^2}\int d^2b\,d^2r\,e^{-i\boldsymbol{k}\cdot\boldsymbol{r}}\,\mathrm{Tr}\langle \boldsymbol{A}^{WW}(\boldsymbol{0})\cdot\boldsymbol{A}^{WW}(\boldsymbol{r})\rangle$$

$$=\frac{4C_F}{\alpha_s(2\pi)^3}\int d^2b\,d^2r\,e^{-i\boldsymbol{k}\cdot\boldsymbol{r}}\frac{1}{\boldsymbol{r}^2}$$

$$\times\left(1-e^{-\boldsymbol{r}^2 Q_{s0}^2 \ln(1/r_T\Lambda)/4}\right), \tag{3}$$

where

$$Q_{s0}^2(\boldsymbol{b})=4\pi\alpha_s^2\rho T(\boldsymbol{b}), \tag{4}$$

with ρ the atomic number density in the nucleus with atomic number A, $T(\boldsymbol{b})$ the nuclear profile function, and Λ some infrared cutoff.

Generalizing Eq. (3) to include nonlinear small-x evolution in it [35–38] is rather difficult. However, the problem of including small-x evolution has been solved for the F_2 structure function and for the gluon production cross section in DIS [35,42]. Inspired by those examples we conjecture that replacing the Glauber-Mueller [46] forward gluon dipole amplitude on the nucleus by its fully evolved expression to be found from the nonlinear evolution equation [35,38]

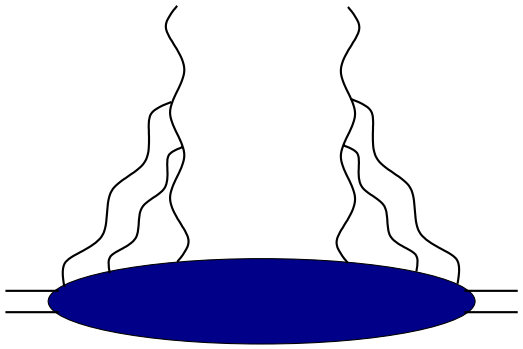

FIG. 2. Definition of the unintegrated gluon distribution in the McLerran-Venugopalan model.

$$1-e^{-r^2Q_{s0}^2\ln(1/r_T\Lambda)/4}\Rightarrow N_G(\boldsymbol{r},\boldsymbol{b},y) \tag{5}$$

would give us the unintegrated gluon distribution function of a nucleus in the general case

$$\phi^{WW}(x,\boldsymbol{k}^2)=\frac{4C_F}{\alpha_s(2\pi)^3}\int d^2b\,d^2r\,e^{-i\boldsymbol{k}\cdot\boldsymbol{r}}\frac{1}{\boldsymbol{r}^2}\times N_G(\boldsymbol{r},\boldsymbol{b},y=\ln 1/x). \tag{6}$$

A similar expression for gluon distribution was obtained earlier in [45].

An important observation concerning the two gluon distributions presented above has been made in [42,43]. It was shown that, while the Weizsäcker-Williams gluon distribution of Eq. (6) indeed has a clear physical meaning of counting the number of gluons [13], it is the gluon distribution inspired by k_T factorization and given by Eq. (2) that enters gluon production cross section in pA collisions and in DIS [42,43]. More precisely, the gluon production cross section including the effects of multiple rescatterings and quantum evolution in it can be reduced to a k_T-factorized form [9] with the unintegrated gluon distribution of a nucleus given by Eq. (2) [42]. The authors cannot offer any simple physical explanation of this paradox. Nevertheless we keep both distributions in the discussion below keeping in mind that the first one is more relevant to particle production in pA.

B. k_T dependence: General arguments

Both definitions of unintegrated gluon distribution (2) and (6) have the same high-k_T asymptotics in the quasi-classical approximation [see, e.g., Eq. (3)], which reads

$$\phi_A(x,\boldsymbol{k}^2)=\phi_A^{WW}(x,\boldsymbol{k}^2)=A\,\phi_N(x,\boldsymbol{k}^2)=A\frac{\alpha_s C_F}{\pi}\frac{1}{\boldsymbol{k}^2},\qquad k_T\to\infty, \tag{7}$$

where the index A (N) denotes gluon distribution in a nucleus (nucleon). Therefore the distributions are equivalent at the level of leading twist, i.e., as long as we include only a single rescattering in the dipole amplitude N_G.

In the quasi-classical case of the McLerran-Venugopalan model both gluon distributions obey a sum rule which we are going to prove here for ϕ. From Eq. (2) one can easily infer that

$$\int d^2k\,\phi_A(x,\boldsymbol{k}^2)=\frac{C_F}{\alpha_s(2\pi)}\int d^2b\,\left[\nabla_r^2 N_G(\boldsymbol{r},\boldsymbol{b},y=\ln 1/x)\right]\Big|_{\boldsymbol{r}=0}. \tag{8}$$

At very small r_T the dipole cross section N_G in the McLerran-Venugopalan model goes to zero as r_T^2 (color transparency [57]) with the coefficient in the front proportional to $A^{1/3}$. One can see that this is explicitly true for the Glauber-Mueller expression for the dipole cross section N_G [46]

$$N_G(\boldsymbol{r},\boldsymbol{b},y=0)=1-e^{-r^2Q_{s0}^2\ln(1/r_T\Lambda)/4}. \tag{9}$$

For N_G from Eq. (9) we observe that

$$\lim_{r_T\to 0}\left(\nabla_r^2 N_G(\boldsymbol{r},\boldsymbol{b},y=0)-A^{1/3}\nabla_r^2 n_G(\boldsymbol{r},\boldsymbol{b},y=0)\right)=0, \tag{10}$$

where n_G is the gluon dipole cross section on a single nucleon obtained from Eq. (9) by expanding it to the lowest nontrivial order and putting $A=1$. Remembering that

$$\int_A d^2b=A^{2/3}\int_N d^2b \tag{11}$$

we conclude from Eqs. (8) and (10) that in the quasi-classical approximation (see also [29])

$$\int d^2k\,\phi_A(y=0,\boldsymbol{k}^2)=A\int d^2k\,\phi_N(y=0,\boldsymbol{k}^2). \tag{12}$$

Similarly one can show that the Weizsäcker-Williams gluon distribution in Eq. (6) obeys the same sum rule in the quasi-classical approximation

$$\int d^2k\,\phi_A^{WW}(y=0,\boldsymbol{k}^2)=A\int d^2k\,\phi_N^{WW}(y=0,\boldsymbol{k}^2). \tag{13}$$

However, the sum rules of Eqs. (12) and (13) break down when the nonlinear evolution with energy [35,38] is included. To see this we first note that for very small r_T one can use the expression for N_G given by the double logarithmic approximation [50,56,45] (see Sec. IV for details on similar calculations)

$$N_G(r_T\approx 0,\boldsymbol{b},y)=\frac{r_T^2Q_{s0}^2}{8\sqrt{\pi}}\frac{\ln^{1/4}\dfrac{1}{r_TQ_{s0}}}{(2\bar{\alpha}_s y)^{3/4}}e^{2\sqrt{2\bar{\alpha}_s y\ln 1/(r_TQ_{s0})}} \tag{14}$$

with

$$\bar{\alpha}_s=\frac{\alpha_s N_c}{\pi}. \tag{15}$$

Similarly for the proton amplitude n_G we write

$$n_G(r_T\approx 0,\boldsymbol{b},y)=\frac{r_T^2\Lambda^2}{8\sqrt{\pi}}\frac{\ln^{1/4}\dfrac{1}{r_T\Lambda}}{(2\bar{\alpha}_s y)^{3/4}}e^{2\sqrt{2\bar{\alpha}_s y\ln 1/(r_T\Lambda)}}, \tag{16}$$

where now the scale characterizing the proton is given by

$$\Lambda^2=4\pi\alpha_s^2\frac{1}{S_p} \tag{17}$$

with S_p the cross sectional transverse area of the proton. Employing the fact that $Q_{s0}^2=A^{1/3}\Lambda^2$ we can easily see that the amplitudes in Eqs. (14) and (16) do not satisfy the con-

dition of Eq. (10) invalidating the sum rule. In fact using Eqs. (14) and (16) in Eq. (10) gives an inequality

$$\lim_{r_T\to 0}(\nabla_r^2 N_G(\boldsymbol{r},\boldsymbol{b},y=\ln 1/x)-A^{1/3}\nabla_r^2 n_G(\boldsymbol{r},\boldsymbol{b},y=\ln 1/x))<0. \tag{18}$$

Equation (18), together with a similar equation for $N_G/\boldsymbol{r}^2$, turn the sum rules of Eqs. (12) and (13) into inequalities

$$\int d^2k\,\phi_A(x,\boldsymbol{k}^2)\leqslant A\int d^2k\,\phi_N(x,\boldsymbol{k}^2) \tag{19}$$

and

$$\int d^2k\,\phi_A^{WW}(x,\boldsymbol{k}^2)\leqslant A\int d^2k\,\phi_N^{WW}(x,\boldsymbol{k}^2), \tag{20}$$

where the equality is achieved only in the quasi-classical limit. We conclude that while multiple rescatterings of gluons in the McLerran-Venugopalan model preserve the total number of gluons in a nuclear wave function at a given rapidity y, the quantum evolution tends to reduce the number of gluons in the wave function via gluon mergers [9].

To study nuclear modification of the gluonic wave functions let us define the unintegrated gluon distributions ratios as

$$R_A(x,\boldsymbol{k}^2)=\frac{\phi_A(x,\boldsymbol{k}^2)}{A\phi_N(x,\boldsymbol{k}^2)}\quad\text{and}\quad R_A^{WW}(x,\boldsymbol{k}^2)=\frac{\phi_A^{WW}(x,\boldsymbol{k}^2)}{A\phi_N^{WW}(x,\boldsymbol{k}^2)}. \tag{21}$$

The sum rules of Eqs. (12) and (13) imply that, in the quasi-classical approximation, if at some k_T the distribution function $\phi_A^{WW}(y=0,\boldsymbol{k}^2)$ is smaller than $A\phi_N^{WW}(y=0,\boldsymbol{k}^2)$, then at some other k_T it should be bigger than $A\phi_N^{WW}(y=0,\boldsymbol{k}^2)$. Using the definitions (21) one concludes from Eq. (13) that if $R_A^{WW}(y=0,\boldsymbol{k}^2)$ is below 1 at some k_T it is bound to go above 1 at some other k_T (for the same value of x). From Eq. (7) we can conclude that

$$R_A(y=0,\boldsymbol{k}^2),R_A^{WW}(y=0,\boldsymbol{k}^2)\to 1,\quad k_T\to\infty. \tag{22}$$

At the same time, when $k_T\ll Q_{s0}$ the saturation effects become important driving $\phi_A^{WW}(y=0,\boldsymbol{k}^2)$ below $A\phi_N^{WW}(y=0,\boldsymbol{k}^2)$, or, equivalently, making $R_A^{WW}(y=0,\boldsymbol{k}^2)<1$. Therefore, due to the sum rule of Eqs. (12) and (13), somewhere in the region of $k_T\gtrsim Q_{s0}$ the ratio $R_A^{WW}(y=0,\boldsymbol{k}^2)$ should go above one, which corresponds to enhancement or broadening of the k_T distribution of gluons inside the nucleus. The same broadening argument applies to $\phi_A(y=0,\boldsymbol{k}^2)$. We have therefore proved that for both gluon distribution functions calculated in the McLerran-Venugopalan model the effects of saturation and the sum rule (12), (13), while making $R_A(y=0,\boldsymbol{k}^2)<1$ in the infrared, also require an existence of a k_T region where $R_A(y=0,\boldsymbol{k}^2)$ is above 1. This conclusion will be quantified in the next section.

The above argument does not apply to the shadowing ratios $R_A(x,\boldsymbol{k}^2)$ and $R_A^{WW}(x,\boldsymbol{k}^2)$ when the effects of quantum evolution are included. The sum rules (12) and (13) are replaced by inequalities (19) and (20) which only require a reduction of the overall number of gluons in the nuclear wave function at a given rapidity y.

C. k_T dependence: Quasi-classical approximation

To investigate the k_T dependence of the unintegrated nuclear gluon distributions $\phi_A^{WW}(x,\boldsymbol{k}^2)$ and $\phi_A(x,\boldsymbol{k}^2)$ more quantitatively and demonstrate the differences of the two distributions let us study them in the McLerran-Venugopalan model [12,13]. For that we take the gluon dipole amplitude in the Glauber-Mueller approximation [46] of Eq. (9). The high-k_T asymptotic for both $\phi_A^{WW}(x,\boldsymbol{k}^2)$ and $\phi_A(x,\boldsymbol{k}^2)$ is given by Eq. (7).

Inside the saturation region ($k_T\ll Q_{s0}$) one has

$$\phi(x,\boldsymbol{k}^2)\approx\frac{2C_FS_A}{\alpha_s(2\pi)^2}\frac{k_T^2}{Q_{s0}^2},\quad k_T\ll Q_{s0} \tag{23}$$

and

$$\phi^{WW}(x,\boldsymbol{k}^2)\approx\frac{4C_FS_A}{\alpha_s(2\pi)^2}\ln\frac{Q_{s0}}{k_T},\quad k_T\ll Q_{s0}, \tag{24}$$

where we assumed for simplicity that the nucleus is cylindrical in which case its cross sectional area is $S_A=\pi\mathcal{R}^2$ and Q_{s0} is given by Eq. (4) with $\rho T(\boldsymbol{b})=A/S_A$:

$$Q_{s0}^2=\frac{4\pi\alpha_s^2A}{S_A},\quad\text{cylindrical nucleus.} \tag{25}$$

In Eqs. (23) and (24) the difference between the two gluon distribution functions becomes manifest: $\phi_A^{WW}(x,\boldsymbol{k}^2)$ keeps increasing (though only logarithmically) as k_T decreases, while $\phi_A(x,\boldsymbol{k}^2)$ turns over and goes to zero in the infrared. Still for both distribution functions the ratio R_A goes to zero as $k_T\to 0$ since to obtain R_A one has to divide Eqs. (23) and (24) by $A\phi_N(x,\boldsymbol{k}^2)$ from Eq. (7). The sum rules (13) and (12) require a region of enhancement ($R_A>1$) at $k_T\gtrsim Q_{s0}$. To see that the enhancement really happens one has to calculate the next-to-leading twist correction to the high-k_T asymptotic of Eq. (7). This technique has been applied previously for quark production in [58]. One obtains

$$\phi_A(x,\boldsymbol{k}^2)=\frac{C_FS_AQ_{s0}^2}{\alpha_s(2\pi)^2\boldsymbol{k}^2}\times\left[1+2\frac{Q_{s0}^2}{\boldsymbol{k}^2}\left(\ln\frac{\boldsymbol{k}^2}{4\Lambda^2}+2\gamma-3\right)+\cdots\right],\ k_T\to\infty \tag{26}$$

and

$$\phi_A^{WW}(x,\boldsymbol{k}^2)=\frac{C_FS_AQ_{s0}^2}{\alpha_s(2\pi)^2\boldsymbol{k}^2}\times\left[1+\frac{Q_{s0}^2}{\boldsymbol{k}^2}\left(\ln\frac{k_T}{2\Lambda}+\gamma-1\right)+\cdots\right],\ k_T\to\infty, \tag{27}$$

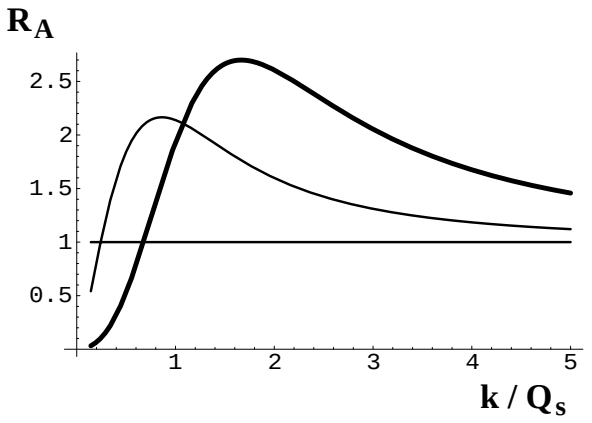

FIG. 3. The ratio R_A of unintegrated gluon distributions in the nucleus and in the nucleon. The thin line represents the Weizsäcker-Williams gluon distribution [Eq. (6)] while the thick line corresponds to the more conventional one inspired by k_T factorization [Eq. (2)].

with γ the Euler constant. For the ratios R_A's this implies

$$R_A = 1 + 2\frac{Q_{s0}^2}{\boldsymbol{k}^2}\left(\ln\frac{\boldsymbol{k}^2}{4\Lambda^2} + 2\gamma - 3\right) + \cdots \tag{28}$$

and

$$R_A^{WW} = 1 + \frac{Q_{s0}^2}{\boldsymbol{k}^2}\left(\ln\frac{k_T}{2\Lambda} + \gamma - 1\right) + \cdots . \tag{29}$$

Therefore the ratios of gluon distributions approach 1 from above for both distribution functions at large k_T. This of course indicates the presence of high-k_T enhancement.

Qualitative plots of ratio R_A for both distribution functions in the McLerran-Venugopalan model are shown in Fig. 3. The thin line corresponds to Weizsäcker-Williams gluon distribution $\phi_A^{WW}(x,\boldsymbol{k}^2)$ while the thick one represents the k_T-factorization distribution $\phi_A(x,\boldsymbol{k}^2)$. One can see that in accordance with Eqs. (23) and (24) the distribution $\phi_A(x,\boldsymbol{k}^2)$ goes to zero faster than $\phi_A^{WW}(x,\boldsymbol{k}^2)$ as $k_T \to 0$ in Fig. 3. In agreement with Eqs. (29) and (28) R_A for the distribution $\phi_A(x,\boldsymbol{k}^2)$ has a stronger high-k_T enhancement than R_A^{WW} for the distribution $\phi_A^{WW}(x,\boldsymbol{k}^2)$.

Finally, let us point out that the function $R_A(R_A^{WW})$ shown in Fig. 3 will be modified when quantum evolution is included. Due to the inequalities of Eqs. (19) and (20) the total number of gluons will decrease. As we will see below in Sec. IV the effects of quantum evolution is to introduce suppression of gluons at all k_T.

III. QUASI-CLASSICAL APPROXIMATION: CRONIN EFFECT ONLY

A. Gluon production in *pA*

The problem of gluon production in proton-nucleus collisions in the quasi-classical approximation (McLerran-Venugopalan model) has been solved in [29] (see also [30,33,31,32]). For a quark-nucleus scattering the production cross section reads [29]

$$\frac{d\sigma^{pA}}{d^2k\,dy} = \int d^2b\,d^2x\,d^2y \frac{1}{(2\pi)^2}\frac{\alpha_s C_F}{\pi^2}\frac{\boldsymbol{x}\cdot\boldsymbol{y}}{\boldsymbol{x}^2\boldsymbol{y}^2}e^{-i\boldsymbol{k}\cdot(\boldsymbol{x}-\boldsymbol{y})} \times\left(1 - e^{-\boldsymbol{x}^2 Q_{s0}^2 \ln(1/x_T\Lambda)/4} - e^{-\boldsymbol{y}^2 Q_{s0}^2 \ln(1/y_T\Lambda)/4} + e^{-(\boldsymbol{x}-\boldsymbol{y})^2 Q_{s0}^2 \ln[1/(\boldsymbol{x}-\boldsymbol{y})_T\Lambda]/4}\right), \tag{30}$$

which then has to be convoluted with the light cone wave function of a quark in a proton. The saturation scale Q_{s0}^2 in Eq. (30) is given by Eq. (4). As was shown in [29] in the approximation when the logarithmic dependence of exponential factors in Eq. (30) on the transverse size is neglected, $\boldsymbol{x}^2\ln(1/x_T\Lambda) \approx \boldsymbol{x}^2$, the $x_\perp$ and $y_\perp$ integrations in Eq. (30) can be done exactly yielding

$$\frac{d\sigma^{pA}}{d^2k\,dy} = \frac{\alpha_s C_F}{\pi^2}\int d^2b\left\{-\frac{1}{\boldsymbol{k}^2} + \frac{2}{\boldsymbol{k}^2}e^{-\boldsymbol{k}^2/Q_{s0}^2} + \frac{1}{Q_{s0}^2}e^{-\boldsymbol{k}^2/Q_{s0}^2}\left[\ln\frac{Q_{s0}^4}{4\Lambda^2\boldsymbol{k}^2} + \mathrm{Ei}\left(\frac{\boldsymbol{k}^2}{Q_{s0}^2}\right)\right]\right\}, \tag{31}$$

where $\mathrm{Ei}(x)$ is the exponential integral. Our goal is to construct the ratio of the number of gluons produced in a *pA* collision over the number of gluons produced in a *pp* collision scaled by the number of collisions

$$R^{pA}(\boldsymbol{k},y) = \frac{\dfrac{d\sigma^{pA}}{d^2k\,dy}}{A\dfrac{d\sigma^{pp}}{d^2k\,dy}}. \tag{32}$$

In the same approximation in which Eq. (31) is derived the gluon production cross section in *pp* scaled up by A is given by

$$A\frac{d\sigma^{pp}}{d^2k\,dy} = \frac{\alpha_s C_F}{\pi^2}\int_A d^2b\frac{Q_{s0}^2}{\boldsymbol{k}^4}, \tag{33}$$

which can be obtained, for instance, by taking the $k_T/Q_{s0} \gg 1$ limit of Eq. (31) and using the fact that $Q_{s0}^2 \sim A^{1/3}$. For a cylindrical nucleus the impact parameter $\boldsymbol{b}$ integration would just give a factor of S_A. Using Eqs. (31) and (33) in Eq. (32) we then obtain

$$R^{pA}(k_T) = \frac{\boldsymbol{k}^4}{Q_{s0}^2}\left\{-\frac{1}{\boldsymbol{k}^2} + \frac{2}{\boldsymbol{k}^2}e^{-\boldsymbol{k}^2/Q_{s0}^2} + \frac{1}{Q_{s0}^2}e^{-\boldsymbol{k}^2/Q_{s0}^2}\left[\ln\frac{Q_{s0}^4}{4\Lambda^2\boldsymbol{k}^2} + \mathrm{Ei}\left(\frac{\boldsymbol{k}^2}{Q_{s0}^2}\right)\right]\right\}. \tag{34}$$

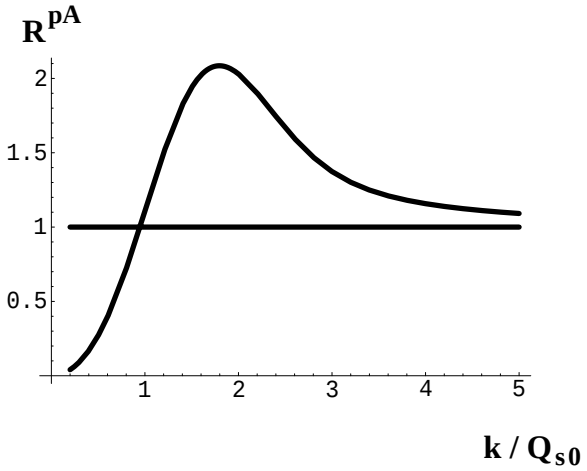

FIG. 4. The ratio R^{pA} for gluons plotted as a function of k_T/Q_{s0} in the quasi-classical McLerran-Venugopalan model as found in [29]. The cutoff is $\Lambda=0.2Q_s$.

The ratio $R^{pA}(k_T)$ is plotted in Fig. 4 for $\Lambda=0.2\ Q_{s0}$. It clearly exhibits an enhancement at high-k_T typical of the Cronin effect [47]. Similar conclusions regarding formula (30) have been reached earlier in [48].

It is worth noting that expanding $R^{pA}(k)$ from Eq. (34) in the powers of Q_{s0}/k_T (''twists'') yields a series with only positive terms

$$R^{pA}(k_T)=1+2\frac{Q_{s0}^2}{\boldsymbol{k}^2}+6\frac{Q_{s0}^4}{\boldsymbol{k}^4}+24\frac{Q_{s0}^6}{\boldsymbol{k}^6}+\cdots=\sum_{n=0}^{\infty}n!\left(\frac{Q_{s0}^2}{\boldsymbol{k}^2}\right)^n. \tag{35}$$

The series (35) is divergent, but it is Borel resummable with the sum given by Eq. (34), though not all terms in Eq. (34) can be reconstructed by the Borel resummation procedure.

To establish whether inclusion of the correct transverse size dependence in the exponents of Eq. (30) would change the conclusion about the Cronin effect let us study the high-k_T asymptotic of Eq. (30). A simple calculation yields

$$\frac{d\sigma^{pA}}{d^2kdy}=\frac{\alpha_sC_F}{\pi^2}\int d^2b\frac{Q_{s0}^2}{\boldsymbol{k}^4}\left[\left(\ln\frac{\boldsymbol{k}^2}{4\Lambda^2}+2\gamma-1\right)+\frac{Q_{s0}^2}{4\boldsymbol{k}^2}\left(6\ln^2\frac{\boldsymbol{k}^2}{4\Lambda^2}-8(4-3\gamma)\ln\frac{\boldsymbol{k}^2}{4\Lambda^2}+29+24\gamma^2-64\gamma\right)+\ldots\right],\quad k_T\to\infty. \tag{36}$$

For a cylindrical nucleus, keeping only the leading logarithmic $[\ln(\boldsymbol{k}^2/\Lambda^2)]$ terms in the parentheses of Eq. (36) we obtain

$$R^{pA}(k_T)=1+\frac{3}{2}\frac{Q_{s0}^2}{\boldsymbol{k}^2}\ln\frac{\boldsymbol{k}^2}{\Lambda^2}+\cdots,\quad k_T\to\infty \tag{37}$$

indicating that R^{pA} approaches 1 from above at high k_T, which is typical of Cronin enhancement. We therefore conclude that in the framework of the quasi-classical approximation employed in [29] the ratio R^{pA} is less than 1 at small $k_T\lesssim Q_{s0}$ and has Cronin enhancement at high $k_T\gtrsim Q_{s0}$.

As can be seen from Eqs. (34) and (37), the position of the Cronin maximum is determined by the saturation scale, such that $k_{\max}=\beta Q_{s0}$, where β is some weakly increasing function of $\ln Q_{s0}/\Lambda$. The height of the maximum is given by $R^{pA}(k_{\max})=R^{pA}(\beta Q_{s0})$. Substituting $k_T=\beta Q_{s0}$ in Eq. (34) we observe that the height of the Cronin maximum scales like

$$R^{pA}(\beta Q_{s0})\sim\ln\frac{Q_{s0}}{\Lambda}+\text{const}\sim\ln A+\text{const}'. \tag{38}$$

Since, for realistic off-central collisions A is replaced by the number of participants N_{part}, we conclude from Eq. (38) that in the quasi-classical approximation considered here the k_T-position and the height of the Cronin peak should increase with centrality of the pA collision.

B. k_T factorization

Let us now show that it is possible to rewrite Eq. (30) in a k_T-factorized form [9,43,42]. Repeating the steps outlined in Sec. IV of [42] we first perform one of the transverse coordinate integrations in Eq. (30) rewriting it as

$$\frac{d\sigma^{pA}}{d^2kdy}=\frac{1}{2\pi^2}\frac{\alpha_sC_F}{\pi}\int d^2bd^2ze^{-i\boldsymbol{k}\cdot\boldsymbol{z}}\times\left[2i\frac{\boldsymbol{z}\cdot\boldsymbol{k}}{\boldsymbol{z}^2\boldsymbol{k}^2}-\ln\frac{1}{z_T\Lambda}\right]N_G(\boldsymbol{z},\boldsymbol{b},0), \tag{39}$$

where $N_G(\boldsymbol{z},\boldsymbol{b},0)$ is given by Eq. (9). Using the fact that $N_G(z=0,\boldsymbol{b},0)=0$ we write Eq. (39) as

$$\frac{d\sigma^{pA}}{d^2kdy}=\frac{1}{2\pi^2}\frac{\alpha_sC_F}{\pi}\frac{1}{\boldsymbol{k}^2}\int d^2bd^2z\times N_G(\boldsymbol{z},\boldsymbol{b},0)\nabla_z^2\left(e^{-i\boldsymbol{k}\cdot\boldsymbol{z}}\ln\frac{1}{z_T\Lambda}\right). \tag{40}$$

Let us denote the forward scattering amplitude of a gluon dipole of transverse size $\boldsymbol{r}$ on a single nucleon (proton) integrated over the impact parameter $\boldsymbol{b}'$ of the dipole measured with respect to the proton by

$$\int d^2b'n_G(\boldsymbol{r},\boldsymbol{b}',y=0)=\pi\alpha_s^2\boldsymbol{r}^2\ln\frac{1}{r_T\Lambda}. \tag{41}$$

Equation (41) is obtained by expanding Eq. (9) at the leading order and taking $A=1$. It corresponds to the two gluon exchange interaction between the dipole and the proton. In the quasi-classical Glauber-Mueller approximation in which Eq. (9) is derived each nucleon exchanges only two gluons with the dipole [46,13]. Therefore Eq. (41) is a natural reduction of Eq. (9) to a single nucleon case.

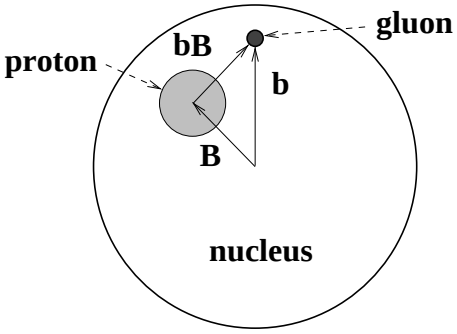

FIG. 5. Gluon production in *pA* collisions as seen in the transverse plane. To make the picture easier to read the gluon is placed far away from the proton which is highly unlikely to happen in real life.

With the help of Eq. (41) we rewrite Eq. (40) as [42]

$$\frac{d\sigma^{pA}}{d^2k dy} = \frac{C_F}{\alpha_s \pi (2\pi)^3} \frac{1}{\boldsymbol{k}^2} \int d^2B d^2b d^2z \times \nabla_z^2 n_G(\boldsymbol{z}, \boldsymbol{b}-\boldsymbol{B}, 0) e^{-i\boldsymbol{k}\cdot\boldsymbol{z}} \nabla_z^2 N_G(\boldsymbol{z}, \boldsymbol{b}, 0). \quad (42)$$

Now $\boldsymbol{B}$ is the impact parameter of the proton with respect to the center of the nucleus and $\boldsymbol{b}$ is the impact parameter of the gluon with respect to the center of the nucleus as shown in Fig. 5.

Equation (42) is the expression for gluon production one would write in the k_T-factorization approach [43]. To see this explicitly let us rewrite Eq. (42) in terms of the unintegrated gluon distribution function from Eq. (2). One easily derives

$$\frac{d\sigma^{pA}}{d^2k dy} = \frac{2\alpha_s}{C_F} \frac{1}{\boldsymbol{k}^2} \int d^2q \, \phi_p(\boldsymbol{q}) \phi_A(\boldsymbol{k}-\boldsymbol{q}), \quad (43)$$

which is the same formula as obtained in the k_T-factorization approach [9,50,43]. ϕ_p is defined as unintegrated gluon distribution of the proton given by Eq. (2) with n_G instead of N_G on the right-hand side. Equation (43) demonstrates that the gluon production cross section in *pA* can be expressed in terms of the gluon distribution (2) in a rather straightforward way [42]. Somehow it is the distribution (2) and not the Weizsäcker-Williams distribution (6) that enters Eq. (43).

Equation (43) demonstrates that, at least in the framework of the McLerran-Venugopalan model, the multiple rescattering leading to Cronin enhancement in *pA* can be incorporated in the gluon distribution functions [29,33]. There is no clear distinction between the nuclear wave function effects and the Glauber-type rescatterings in the nucleus. Antishadowing present in the gluon distribution function $\phi_A(\boldsymbol{k})$ as shown in Fig. 3 simply translates into the Cronin effect of Fig. 4 via Eq. (43).

In the quasi-classical approximation of the McLerran-Venugopalan model one can prove a sum rule for the gluon production cross section in *pA* similar to the sum rule we proved for gluon distributions in Sec. II B. To prove the sum rule we note that Eq. (42) implies that

$$\int d^2k \boldsymbol{k}^2 \frac{d\sigma^{pA}}{d^2k dy} = \frac{C_F}{\alpha_s 2\pi^2} \int d^2B d^2b [\nabla_z^2 n_G(\boldsymbol{z}, \boldsymbol{b}-\boldsymbol{B}, 0)]|_{z=0} \times [\nabla_z^2 N_G(\boldsymbol{z}, \boldsymbol{b}, 0)]|_{z=0}. \quad (44)$$

For Glauber-Mueller N_G from Eq. (9) and for n_G from Eq. (41) the following condition is satisfied:

$$\lim_{z_T \to 0} \{ [\nabla_z^2 n_G(\boldsymbol{z}, \boldsymbol{b}-\boldsymbol{B}, 0)][\nabla_z^2 N_G(\boldsymbol{z}, \boldsymbol{b}, 0)] - A^{1/3} [\nabla_z^2 n_G(\boldsymbol{z}, \boldsymbol{b}-\boldsymbol{B}, 0)][\nabla_z^2 n_G(\boldsymbol{z}, \boldsymbol{b}, 0)] \} = 0. \quad (45)$$

The impact parameter integration in *pA* will give an extra factor of $A^{2/3}$ as compared to *pp*. Together with Eq. (45) this gives

$$\int d^2k \boldsymbol{k}^2 \frac{d\sigma_{MV}^{pA}}{d^2k dy} = A \int d^2k \boldsymbol{k}^2 \frac{d\sigma_{MV}^{pp}}{d^2k dy} \quad (46)$$

in the quasi-classical approximation.

Similar to the sum rule proved in Sec. II for gluon distribution functions, the sum rule (46) insures that if the quasi-classical gluon production cross section in *pA* collisions is, in some region of k_T, smaller than A times the gluon production cross section in *pp* than there should be some other region of k_T in which their roles are reversed. For R^{pA} defined in Eq. (32) that means that if, in some region of k_T, it is less than 1 there must be some other region of k_T in which it is greater than 1. Of course the $\boldsymbol{k}^2$ factors in Eq. (46) make the quantitative amounts of suppression and enhancement very different from the ones dictated by, for instance, the sum rule of Sec. II.

In the quasi-classical approximation for the gluon production in *pA* considered above R^{pA} is below 1 at $k_T \lesssim Q_{s0}$. Expanding Eq. (34) for $k_T \ll Q_{s0}$ we write

$$R^{pA}(k) \approx \frac{\boldsymbol{k}^2}{Q_{s0}^2} \ll 1 \quad \text{if} \quad k_T \ll Q_{s0}. \quad (47)$$

Equation (47), together with the sum rule (46) imply that there must exist a region of k_T with a Cronin-like enhancement of gluon production, which is demonstrated by the full answer plotted in Fig. 4.

IV. INCLUDING SMALL-x EVOLUTION: SUPPRESSION AT ALL p_T

A. Including small-x evolution

As the energy of the collisions increases quantum evolution corrections become important. For produced particles with the same k_T higher energy implies a smaller effective Bjorken x meaning that the quantum corrections of the type $\alpha_s \ln 1/x$ should be resummed. These corrections can be resummed by the Balitsky-Fadin-Kuraev-Lipatov (BFKL) equation [34], which calculates the contribution of the hard (perturbative) Pomeron. However, as energy increases multiple Pomeron exchanges become important, resulting in a

more complicated small-x evolution [39,40]. In [35,38] an equation was constructed which resums multiple Pomeron exchanges for a forward amplitude of a $q\bar{q}$ dipole scattering on a nucleus in the large N_c limit. The forward amplitude $N(\boldsymbol{r},\boldsymbol{b},Y)$ of a dipole of transverse size $\boldsymbol{r}$ scattering at impact parameter $\boldsymbol{b}$ and rapidity Y was normalized such that the total $q\bar{q}A$ cross section was given by

$$\sigma_{\rm tot}^{q\bar{q}A}=2\int d^2bN(\boldsymbol{r},\boldsymbol{b},Y). \tag{48}$$

The evolution equation for $N(\boldsymbol{r},\boldsymbol{b},Y)$ closes only in the large-N_c limit of QCD [38,39] and reads [35–37]

$$\begin{aligned}N(\boldsymbol{x}_{01},\boldsymbol{b},Y)=&N(\boldsymbol{x}_{01},\boldsymbol{b},Y=0)e^{-(4\alpha C_F/\pi)\ln(x_{01}/\rho)Y}\\&+\frac{\alpha C_F}{\pi^2}\int_0^Y dy e^{-(4\alpha C_F/\pi)\ln(x_{01}/\rho)(Y-y)}\\&\times\int_\rho d^2x_2\frac{x_{01}^2}{x_{02}^2x_{12}^2}\Big[2N\Big(\boldsymbol{x}_{02},\boldsymbol{b}+\frac{1}{2}\boldsymbol{x}_{12},y\Big)\\&-N\Big(\boldsymbol{x}_{02},\boldsymbol{b}+\frac{1}{2}\boldsymbol{x}_{12},y\Big)N\Big(\boldsymbol{x}_{12},\boldsymbol{b}+\frac{1}{2}\boldsymbol{x}_{02},y\Big)\Big],\end{aligned} \tag{49}$$

with the initial condition given by $N(\boldsymbol{x}_{01},\boldsymbol{b},Y=0)$ taken to be of Mueller-Glauber form [46] in [35]:

$$N(\boldsymbol{x}_{01},\boldsymbol{b}_0,Y=0)=1-e^{-x_{01}^2Q_{0s}^{\rm quark\ 2}\ln(1/x_{01T}\Lambda)/4}, \tag{50}$$

where

$$N_cQ_{0s}^{\rm quark\ 2}=C_FQ_{s0}^2. \tag{51}$$

In [42] it was shown how to resum the effects of nonlinear evolution of Eq. (49) for gluon production in DIS. In the quasi-classical approximation the gluon production in DIS is given by a formula similar to Eq. (30) [44]. That formula can also be recast in a k_T factorized form of Eq. (42) [42]. As was proven in [42] in order to include quantum evolution (49) in Eq. (42) for DIS one has to make replacements. First, one has to replace $N_G(\boldsymbol{z},\boldsymbol{b},0)$ in Eq. (42) by the forward quark dipole amplitude using the following expression valid in the large-N_c limit [42]:

$$N_G(\boldsymbol{z},\boldsymbol{b},y)=2N(\boldsymbol{z},\boldsymbol{b},y)-N(\boldsymbol{z},\boldsymbol{b},y)^2, \tag{52}$$

where $N(\boldsymbol{z},\boldsymbol{b},y)$ is the forward scattering amplitude of a $q\bar{q}$ dipole on a nucleus evolved by nonlinear equation (49). Then one has to replace $n_G(\boldsymbol{z},\boldsymbol{b},0)$ by $n_G(\boldsymbol{z},\boldsymbol{b},Y-y)$ evolved just by the linear part of Eq. (49) (the BFKL equation [34]). Here Y is the total rapidity interval between the projectile (virtual photon) and target nucleus in a DIS collision. The initial conditions for both N_G and n_G evolution are given by $N_G(\boldsymbol{z},\boldsymbol{b},0)$ and $n_G(\boldsymbol{z},\boldsymbol{b},0)$ correspondingly.

Since both pA and DIS are considered here as scatterings of an unsaturated projectile (proton or $q\bar{q}$ pair) on a saturated target (nucleus) with the gluon production in the quasi-classical limit given by the same Eq. (42), we may conjecture that inclusion of quantum evolution (49) in a gluon production cross section is done similarly for both processes. We therefore write

$$\begin{aligned}\frac{d\sigma^{pA}}{d^2kdy}=&\frac{C_F}{\alpha_s\pi(2\pi)^3}\frac{1}{\boldsymbol{k}^2}\int d^2Bd^2bd^2z\\&\times\nabla_z^2n_G(\boldsymbol{z},\boldsymbol{b}-\boldsymbol{B},Y-y)e^{-i\boldsymbol{k}\cdot\boldsymbol{z}}\nabla_z^2N_G(\boldsymbol{z},\boldsymbol{b},y),\end{aligned} \tag{53}$$

where Y is the total rapidity interval between the proton and the nucleus. Just like in DIS N_G in Eq. (53) is given by Eq. (52), where N should be found from Eq. (49), while n_G should be determined from the linear part of Eq. (53) (BFKL) with the initial conditions given by Eq. (41). Equation (53) is exact if the proton is modeled as a diquark–quark pair [59], in which case it would be identical to a $q\bar{q}$ pair produced by a virtual photon in DIS. In the general case Eq. (53) remains a well-motivated conjecture.

As in Sec. II the sum rule (46) breaks down once nonlinear evolution [35,38] is included in the way shown in Eq. (53). Using the double logarithmic expressions (14) and (16) modifies Eq. (45) into

$$\begin{aligned}\lim_{z_T\to0}\{&[\nabla_z^2n_G(\boldsymbol{z},\boldsymbol{b}-\boldsymbol{B},Y-y)][\nabla_z^2N_G(\boldsymbol{z},\boldsymbol{b},y)]\\&-A^{1/3}[\nabla_z^2n_G(\boldsymbol{z},\boldsymbol{b}-\boldsymbol{B},Y-y)][\nabla_z^2n_G(\boldsymbol{z},\boldsymbol{b},y)]\}<0\end{aligned} \tag{54}$$

turning the sum rule of Eq. (46) into an inequality for the cross section from Eq. (53)

$$\int d^2k\boldsymbol{k}^2\frac{d\sigma^{pA}}{d^2kdy}\leqslant A\int d^2k\boldsymbol{k}^2\frac{d\sigma^{pp}}{d^2kdy}. \tag{55}$$

Again the effect of quantum evolution is to reduce the total number of gluons at a given rapidity, though now it is shown for the case of gluon production weighted by k_T^2. Let us now study in detail how this suppression sets in for various regions of k_T.

In the following we are going to study effects of evolution equation (49) on the gluon spectrum and on R^{pA}. Our goal is to determine whether R^{pA} preserves the shape shown in Fig. 4 with the Cronin maximum and low-k_T suppression, or quantum evolution would modify this shape introducing extra suppression. Below we will first study the effects of quantum evolution at high-k_T, $k_T\gtrsim Q_s$, showing that evolution introduces suppression ($R^{pA}<1$) in that region. We will then proceed by studying the fate of the Cronin peak ($k_T\sim Q_s$) as evolution sets in. We will show that the Cronin maximum will decrease with the onset of evolution and would eventually disappear. We will then argue that suppression persists for $k_T\ll Q_s$ when evolution effects are included. We will end the section by constructing a toy model summarizing our conclusions.

To simplify the discussion we will consider a cylindrical nucleus for which Eq. (53) reduces to

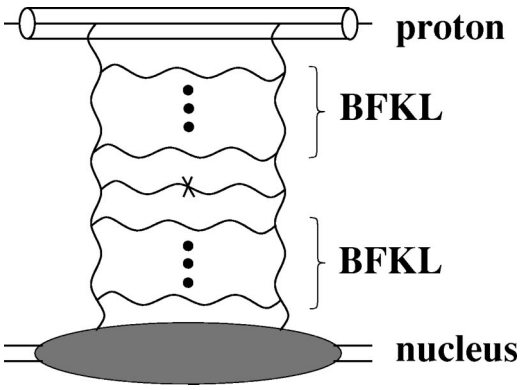

FIG. 6. Gluon production in *pA* collisions at the leading twist level (see text).

$$\frac{d\sigma^{pA}}{d^2k\,dy}=\frac{C_F}{\alpha_s\pi(2\pi)^3}\frac{S_pS_A}{\boldsymbol{k}^2}\int d^2z \times\nabla_z^2 n_G(\boldsymbol{z},Y-y)e^{-i\boldsymbol{k}\cdot\boldsymbol{z}}\nabla_z^2 N_G(\boldsymbol{z},y), \tag{56}$$

with S_p the cross sectional area of the proton.

B. Leading twist effects

1. Leading twist gluon production cross section

We start by exploring the leading high-k_T behavior of the gluon spectrum given by Eq. (56). At very high k_T the integral in Eq. (56) is dominated by small values of z_T. Therefore we can neglect the quadratic term in the evolution equation for N_G (49) leaving only the linear part—the BFKL evolution with initial conditions for a gluon dipole given by Eq. (9). The corresponding Feynman diagram is shown in Fig. 6. The solution of the BFKL equation is well-known and reads

$$N_{G1}(\boldsymbol{z},y)=\int\frac{d\lambda}{2\pi i}C_\lambda^A(z_TQ_{s0})^\lambda e^{2\bar{\alpha}_s\chi(\lambda)y} \tag{57}$$

with

$$\chi(\lambda)=\psi(1)-\frac{1}{2}\psi\left(1-\frac{\lambda}{2}\right)-\frac{1}{2}\psi\left(\frac{\lambda}{2}\right), \tag{58}$$

with $\bar{\alpha}_s$ defined in Eq. (15) and Q_{s0} for a cylindrical nucleus given by Eq. (25). The coefficient C_λ^A is fixed from the initial conditions at $y=0$ given by Eq. (9). Then for small $z_T<1/Q_{s0}$

$$C_\lambda^A=\sum_{n=1}^{\infty}\sum_{m=0}^{n}\frac{(-1)^{n+1}}{4^n(n-m)!(2n-\lambda)^{m+1}}\ln^{n-m}\frac{Q_{s0}}{\Lambda} =\sum_{n=1}^{\infty}\frac{1}{4^n n!(\lambda-2n)^{n+1}}\left(\frac{Q_{s0}}{\Lambda}\right)^{2n-\lambda} \times\Gamma\left(1+n,(2n-\lambda)\ln\frac{Q_{s0}}{\Lambda}\right). \tag{59}$$

Similarly for the gluon dipole cross section on the proton we write

$$n_G(\boldsymbol{z},y)=\int\frac{d\lambda}{2\pi i}C_\lambda^p(z_T\Lambda)^\lambda e^{2\bar{\alpha}_s\chi(\lambda)y}, \tag{60}$$

where the scale characterizing the proton Λ is given by Eq. (17). The coefficient C_λ^p is obtained by requiring that Eq. (60) reduces to Eq. (41) when $y=0$. For $z_T<1/\Lambda$ we derive

$$C_\lambda^p=\frac{1}{4(\lambda-2)^2}. \tag{61}$$

[We have identified the nonperturbative scale characterizing the proton (17) with the infrared cutoff employed earlier in Eq. (41).]

Substituting Eqs. (57) and (60) into Eq. (56) and integrating over $\boldsymbol{z}$ yields [60,61]

$$\left.\frac{d\sigma^{pA}}{d^2k\,dy}\right|_{LT}=\frac{C_FS_pS_A}{4\alpha_s(2\pi)^3}\int\frac{d\lambda}{2\pi i}\frac{d\lambda'}{2\pi i}\lambda^2\lambda'^2C_\lambda^AC_{\lambda'}^p2^{\lambda+\lambda'} \times\frac{\Gamma\left(-1+\frac{\lambda+\lambda'}{2}\right)}{\Gamma\left(2-\frac{\lambda+\lambda'}{2}\right)}\left(\frac{Q_{s0}}{k_T}\right)^\lambda\left(\frac{\Lambda}{k_T}\right)^{\lambda'} \times e^{2\bar{\alpha}_s[\chi(\lambda)y+\chi(\lambda')(Y-y)]}. \tag{62}$$

Equation (62) gives the leading twist expression for the gluon production cross section in *pA* collisions and is illustrated in Fig. 6.

The difference between Eq. (62) and Eq. (13) of [60] is in gamma functions in the integrand. The difference manifests itself at the order of higher twists, where the gluon distributions used in [60], if taken at $y=0$ and used in inverted Eq. (2) to obtain n_p, would yield higher twist corrections (higher powers of r_T) to the right-hand side of Eq. (41), which should not be there in the two-gluon exchange approximation corresponding to the $y=0$ limit.

2. Double logarithmic approximation: Monojet versus dijet and first signs of high-p_T suppression

To derive the high-k_T behavior of the gluon production cross section in Eq. (62) we have to evaluate the integrals in it by the saddle point method. When $k_T\gg Q_{s0},\Lambda$ we approximately write

$$\chi(\lambda)\approx\frac{1}{2-\lambda}. \tag{63}$$

Then the saddle points are given by

$$\lambda_{sp}=2-\sqrt{\frac{2\bar{\alpha}_sy}{\ln(k_T/Q_{s0})}} \tag{64}$$

and

$$\lambda'_{\rm sp}=2-\sqrt{\frac{2\bar{\alpha}_s(Y-y)}{\ln(k_T/\Lambda)}}. \tag{65}$$

Integrating over λ and λ' around the saddle points (64) and (65) in Eq. (62) yields gluon production cross section in double logarithmic approximation (DLA) [50]

$$\left.\frac{d\sigma^{pA}}{d^2k\,dy}\right|_{\rm DLA}\approx\frac{C_F S_p S_A}{\alpha_s(2\pi)^4}\frac{Q_{s0}^2\Lambda^2}{\boldsymbol{k}^4}\frac{1}{2\bar{\alpha}_s}\left[\frac{\ln\frac{k_T}{Q_{s0}}\ln\frac{k_T}{\Lambda}}{y^3(Y-y)^3}\right]^{1/4}\times\left(\sqrt{\frac{y}{\ln\frac{k_T}{Q_{s0}}}}+\sqrt{\frac{Y-y}{\ln\frac{k_T}{\Lambda}}}\right)\times\exp\left(2\sqrt{2\bar{\alpha}_s y\ln\frac{k_T}{Q_{s0}}}+2\sqrt{2\bar{\alpha}_s(Y-y)\ln\frac{k_T}{\Lambda}}\right). \tag{66}$$

To understand Eq. (66) let us first construct the gluon distribution function

$$xG_A(x,Q^2)=\int_{\Lambda^2}^{Q^2}dk_T^2\,\phi^A(x,\boldsymbol{k}^2) \tag{67}$$

in the same double logarithmic approximation [10]. Using Eq. (57) in Eqs. (2) and (67) we obtain in the double logarithmic approximation

$$xG_A(x,Q^2)=\frac{C_F S_A Q_{s0}^2}{\alpha_s(2\pi)^3}2\sqrt{\pi}\frac{\ln^{1/4}\frac{Q}{Q_{s0}}}{[2\bar{\alpha}_s\ln(1/x)]^{3/4}}\times e^{2\sqrt{2\bar{\alpha}_s\ln(1/x)\ln(Q/Q_{s0})}}. \tag{68}$$

Since the above gluon distribution is obtained in the DLA (large Q^2) limit of the BFKL equation, it can also be obtained by taking the small-x limit of the DGLAP equation [62]. One can explicitly check that with the help of Eq. (68) and an analogous one for the proton gluon distribution xG_p, Eq. (66) can be rewritten as

$$\frac{d\sigma^{pA}}{d^2k\,dy}=\frac{2\alpha_s}{C_F\boldsymbol{k}^2}\left[xG_p(x=e^{-Y+y},\boldsymbol{k}^2)\frac{\partial}{\partial k_T^2}xG_A(x=e^{-y},\boldsymbol{k}^2)+xG_A(x=e^{-y},\boldsymbol{k}^2)\frac{\partial}{\partial k_T^2}xG_p(x=e^{-Y+y},\boldsymbol{k}^2)\right]. \tag{69}$$

Equation (69) can be obtained directly by using Eq. (68) in Eq. (43) and assuming that the q integration in Eq. (43) is dominated by the regions near $\boldsymbol{q}=0$ and $\boldsymbol{q}=\boldsymbol{k}$ [9,50]. As was shown in detail in [11], Eq. (69) can be reduced to

$$\frac{d\sigma^{pA}}{d^2k\,dy}=\frac{2}{\pi N_c C_F}\left(\int_{e^{-Y+y}}^1\frac{dx_1}{x_1}x_1G_p(x_1,\boldsymbol{k}^2)xG_A(x=e^{-y},\boldsymbol{k}^2)+\int_{e^{-y}}^1\frac{dx_1}{x_1}xG_p(x=e^{-Y+y},\boldsymbol{k}^2)\times x_1G_A(x_1,\boldsymbol{k}^2)\right)\frac{d\hat{\sigma}^{gg\to gg}}{d^2k}, \tag{70}$$

which is the standard dijet production cross section derived in the collinear factorization approximation (see, e.g., [11]). [Of course one of the jet's momentum in Eq. (70) is integrated over.] Therefore we have started with a single jet production cross section given by k_T-factorized expression (62) with BFKL gluon distributions and demonstrated that in the large k_T limit it reduces to the conventional dijet production cross section (70) given by collinear factorization with DGLAP-evolved structure functions.[1]

Before we continue let us study R^{pA} given by the cross section of Eq. (66). The naive expectation for the high-k_T limit of the leading twist gluon production cross section would be that $R^{pA}=1$. However, already at the level of approximation employed in Eq. (66) this is not quite the case. To see this let us first write down an expression for the gluon production cross section in pp collisions in the leading twist DLA approximation. It is obtained by replacing Q_{s0} and S_A in Eq. (66) by Λ and S_p correspondingly. We obtain

$$\left.\frac{d\sigma^{pp}}{d^2k\,dy}\right|_{\rm DLA}\approx\frac{C_F S_p^2}{\alpha_s(2\pi)^4}\frac{\Lambda^4}{\boldsymbol{k}^4}\frac{1}{2\bar{\alpha}_s}\frac{\sqrt{y}+\sqrt{Y-y}}{y^{3/4}(Y-y)^{3/4}}\times\exp\left[2\sqrt{2\bar{\alpha}_s\ln\frac{k_T}{\Lambda}}(\sqrt{y}+\sqrt{Y-y})\right]. \tag{71}$$

To calculate R^{pA} we note that since $S_A=A^{2/3}S_p$ one concludes from Eqs. (25) and (17) that $Q_{s0}^2=A^{1/3}\Lambda^2$. Using Eqs. (66) and (71) in Eq. (32) yields

$$R^{pA}(k_T,y)|_{k_T\gg Q_s}=\frac{\left(\ln\frac{k_T}{Q_{s0}}\ln\frac{k_T}{\Lambda}\right)^{1/4}}{\sqrt{y}+\sqrt{Y-y}}\left(\sqrt{\frac{y}{\ln\frac{k_T}{Q_{s0}}}}+\sqrt{\frac{Y-y}{\ln\frac{k_T}{\Lambda}}}\right)\times\exp\left[2\sqrt{2\bar{\alpha}_s y}\left(\sqrt{\ln\frac{k_T}{Q_{s0}}}-\sqrt{\ln\frac{k_T}{\Lambda}}\right)\right], \tag{72}$$

where $Q_s=Q_s(y)$ is the full energy dependent saturation scale, which reduces to Q_{s0} at $y=0$. Defining

[1]We thank Al Mueller for encouraging one of the authors (Yu. K.) to verify this correspondence explicitly several years ago.

$$\xi \equiv \left(\frac{\ln \frac{k_T}{Q_{s0}}}{\ln \frac{k_T}{\Lambda}} \right)^{1/4} \tag{73}$$

we rewrite Eq. (72) as

$$R^{pA}(\xi,y)\Big|_{\xi<1} = \frac{\frac{1}{\xi}\sqrt{y}+\xi\sqrt{Y-y}}{\sqrt{y}+\sqrt{Y-y}} \times \exp\left[-2\sqrt{2\bar{\alpha}_s y \frac{1-\xi^2}{1+\xi^2}\ln\frac{Q_{s0}}{\Lambda}} \right], \tag{74}$$

where $\xi<1$ for $k_T>Q_{s0}$, since $Q_{s0}^2=A^{1/3}\Lambda^2 \gg \Lambda^2$. For the large transverse momenta in question, $k_T \gg Q_s(y)$, the variable ξ is approaching 1 from below as is clear from Eq. (73). In the limit $\xi \to 1$ Eq. (74) becomes

$$\begin{aligned} R^{pA}(\xi,y)\Big|_{\xi\to 1} &\approx \left(1+(1-\xi)\frac{\sqrt{y}-\sqrt{Y-y}}{\sqrt{y}+\sqrt{Y-y}} \right) \\ &\quad \times \exp\left[-2\sqrt{2\bar{\alpha}_s y(1-\xi)\ln\frac{Q_{s0}}{\Lambda}} \right] \\ &< (2-\xi)\exp\left[-2\sqrt{2\bar{\alpha}_s y(1-\xi)\ln\frac{Q_{s0}}{\Lambda}} \right] \\ &\approx \exp\left[-2\sqrt{2\bar{\alpha}_s y(1-\xi)\ln\frac{Q_{s0}}{\Lambda}} \right] \\ &< 1, \quad k_T \gg Q_s(y). \end{aligned} \tag{75}$$

We neglected $2-\xi=1+(1-\xi)$ in front of the exponent in Eq. (75) since the $(1-\xi)$ correction to 1 in it is not enhanced by any parametrically large variables, such as y and $\ln Q_{s0}/\Lambda$ in the exponent. If $R^{pA}(\xi,y)$ from Eq. (75) is expanded in powers of $(1-\xi)$ this prefactor term would give subleading logarithmic corrections to the expansion of the exponent, which are negligible in the DLA limit considered here.

We conclude that R^{pA} from Eq. (72) is smaller than one. Since $R^{pA}(\xi,y)$ in Eq. (75) is an increasing function of ξ and ξ is an increasing function of k_T, we observe that $R^{pA}(k_T,y)$ in Eq. (72) is an increasing function of k_T approaching 1 from below. This suppression is mainly due to the difference of the cutoffs in the logarithms of transverse momentum in the exponent of Eq. (72). The cutoff for the nucleus case is given by the nuclear saturation scale, which is different from the appropriate scale in a single proton. The high momentum regions, where linear evolution equations work, are cut off from below by saturation scales, which are different for different nuclei and for the proton. In this way, as we can see from Eqs. (72) and (75), saturation influences the physics at high k_T as long as corresponding x_{Bj} is small. The effect of saturation is to introduce high-k_T suppression.

The suppression of Eq. (75) is a leading twist effect and is due to quantum evolution. In this sense it is similar to the suppression suggested in [8]. However, the suppression of [8] corresponds to a region of lower k_T, where the double logarithmic approximation of Eq. (72) is not valid anymore. There the suppression happens due to the change in anomalous dimension of the gluon distribution function, as we are going to discuss below.

3. Onset of anomalous dimension: More high-p_T suppression

For the values of k_T lower than considered above (but still much larger than Q_{s0}) the saddle point of λ integration in Eq. (62) shifts to a smaller value than given by Eq. (64). While in determining the saddle point of Eq. (64) we had to expand $\chi(\lambda)$ around $\lambda=2$, now we have to expand it around $\lambda=1$. There one writes

$$\chi(\lambda) \approx 2\ln 2 + \frac{7}{4}\zeta(3)(\lambda-1)^2 \tag{76}$$

obtaining the value of the saddle point

$$\lambda_{\rm sp}^* = 1 + \frac{\ln\frac{k_T}{Q_{s0}}}{7\zeta(3)\bar{\alpha}_s y}. \tag{77}$$

As was suggested in [45], the transition of the saddle point from the value given in Eq. (64) to the one given in Eq. (77) happens around

$$k_{\rm geom} \approx Q_s(y)\frac{Q_s(y)}{Q_{s0}} \tag{78}$$

indicating the onset of a geometric scaling regime [55]. Here in the double logarithmic approximation the saturation scale depends on energy as [56,45,63]

$$Q_s(y) \approx Q_{s0} e^{2\bar{\alpha}_s y}. \tag{79}$$

The precise value of the scale $k_{\rm geom}$ in Eq. (78) depends on the definition of the saturation scale and on the way one defines the transition between the double logarithmic and geometric scaling regions. For instance, if we define the transition by equating the saddle points of Eqs. (64) and (77),

$$\lambda_{\rm sp} = \lambda_{\rm sp}^*, \tag{80}$$

we get at the point of closest approach (the two saddle point values are never equal to each other)

$$k_{\rm geom} = Q_{s0} e^{\bar{\alpha}_s y 7^{2/3}\zeta(3)^{2/3}2^{-1/3}} \approx Q_{s0} e^{3.28\bar{\alpha}_s y}. \tag{81}$$

When combined with the saturation scale from Eq. (79) this gives

$$k_{\rm geom} \approx Q_s(y)\left(\frac{Q_s(y)}{Q_{s0}}\right)^{0.64}, \tag{82}$$

which is slightly different from Eq. (78). At the same time, using the energy dependence of the saturation scale found in [64] in the fixed coupling case

$$Q_s(y) \approx Q_{s0} e^{2.44 \bar{\alpha}_s y} \tag{83}$$

in Eq. (81) gives

$$k_{\rm geom} \approx Q_s(y) \left(\frac{Q_s(y)}{Q_{s0}} \right)^{0.34}, \tag{84}$$

which is even lower than Eq. (82). A definition of the transition point different from Eq. (80) would give slightly different estimates for $k_{\rm geom}$.

Nevertheless, the ambiguities in the scale $k_{\rm geom}$ notwithstanding, one can argue, as was done in [45], that there exists a large momentum scale $k_{\rm geom}$, which is parametrically larger than the saturation scale

$$k_{\rm geom} \gg Q_s(y). \tag{85}$$

For $k_T \gtrsim k_{\rm geom}$ there is no geometric scaling and the gluon production is well described by the double logarithmic approximation described above resulting in R^{pA} from Eq. (72). $k_T \lesssim k_{\rm geom}$ is the region of geometric scaling [45]. When $k_T \lesssim Q_s(y)$ (saturation region) multiple Pomeron exchanges become important leading to the saturation of structure functions [9]. For $Q_s(y) \lesssim k_T \lesssim k_{\rm geom}$ (extended geometric scaling region) multiple Pomeron exchanges are not important yet and the gluon production cross section is described by the leading twist expression in Eq. (62) with the λ-integral evaluated near the saddle point of Eq. (77) [8].

Performing the λ and λ' integrals in Eq. (62) in the saddle point approximation around the saddle points of Eqs. (77) and (65) correspondingly yields

$$\left. \frac{d\sigma^{pA(1)}}{d^2k dy} \right|_{\rm LLA} \approx \frac{C_F S_p S_A}{\alpha_s (2\pi)^4} \frac{Q_{s0} \Lambda^2}{\boldsymbol{k}^3} \frac{C_1^A \ln^{1/4} \frac{k_T}{\Lambda}}{\sqrt{7\zeta(3) \bar{\alpha}_s} (Y-y)^{3/4} (2\bar{\alpha}_s)^{1/4}} \times \exp\left[(\alpha_P - 1) y + 2 \sqrt{2\bar{\alpha}_s (Y-y) \ln \frac{k_T}{\Lambda}} - \frac{\ln^2 \frac{k_T}{Q_{s0}}}{14\zeta(3) \bar{\alpha}_s y} \right], \tag{86}$$

where

$$\alpha_P - 1 = 2\bar{\alpha}_s \ln 2 \tag{87}$$

is the BFKL Pomeron intercept [34] and C_1^A is well-approximated by the first term in the series of Eq. (59) for all physically reasonable values of A,

$$C_1^A \approx \frac{1}{4} \left(1 + \ln \frac{Q_{s0}}{\Lambda} \right) = \frac{1}{4} \left(1 + \frac{1}{6} \ln A \right). \tag{88}$$

The superscript (1) in Eq. (86) denotes the leading twist contribution. We assume that in the transverse momentum region where Eq. (86) is valid, $Q_s(y) \lesssim k_T \lesssim k_{\rm geom}$, the gluon production cross section in pp collisions is still given by Eq. (71). This is a good approximation since if $k_T \gtrsim Q_s(y) \gg \Lambda$ the double logarithmic approximation of Eq. (71) should work. Using Eqs. (86) and (71) in Eq. (32) we obtain

$$R^{pA}(k_T,y)\big|_{Q_s(y) \lesssim k_T \lesssim k_{\rm geom}} = \frac{k_T}{Q_{s0}} \frac{2C_1^A}{\sqrt{7\zeta(3)}} \frac{\ln^{1/4} \frac{k_T}{\Lambda}}{(2\bar{\alpha}_s)^{1/4}} \frac{y^{1/4}}{\sqrt{y} + \sqrt{Y-y}} \times \exp\left[(\alpha_P - 1) y - 2 \sqrt{2\bar{\alpha}_s y \ln \frac{k_T}{\Lambda}} - \frac{\ln^2 \frac{k_T}{Q_{s0}}}{14\zeta(3)\bar{\alpha}_s y} \right]. \tag{89}$$

To determine whether $R^{pA}(k_T,y)$ in Eq. (89) is greater or less than 1 we first drop the slowly varying and constant prefactors in front of the exponent and write

$$R^{pA}(k_T,y)\big|_{Q_s(y) \lesssim k_T \lesssim k_{\rm geom}} \sim \frac{k_T}{Q_{s0}} \exp\left[(\alpha_P - 1) y - 2 \sqrt{2\bar{\alpha}_s y \ln \frac{k_T}{\Lambda}} - \frac{\ln^2 \frac{k_T}{Q_{s0}}}{14\zeta(3)\bar{\alpha}_s y} \right] \tag{90}$$

keeping only parametrically important factors. To estimate the value of R^{pA} in Eq. (90) in the extended geometric scaling region $Q_s(y) \lesssim k_T \lesssim k_{\rm geom}$ we substitute $k_T = k_{\rm geom}$ into Eq. (90) with $k_{\rm geom}$ from Eq. (78). The result yields an asymptotically small value

$$R^{pA}(k_T,y)\big|_{Q_s(y) \lesssim k_T \lesssim k_{\rm geom}} \sim e^{-1.65 \bar{\alpha}_s y} \ll 1, \tag{91}$$

where we used $A = 197$ for the gold nucleus. For other values of A and for other values of k_T in the region $Q_s(y) \lesssim k_T \lesssim k_{\rm geom}$ one still gets exponential suppression for $R^{pA}(k_T,y)$. Therefore we conclude that $R^{pA}(k_T,y) < 1$ in the extended geometric scaling region $Q_s(y) \lesssim k_T \lesssim k_{\rm geom}$.

As can be checked explicitly, for a sufficiently large nucleus (large A), $R^{pA}(k_T,y)$ of Eq. (89) is an increasing function of k for $Q_s(y) \lesssim k_T \lesssim k_{\rm geom}$. As k_T increases it should smoothly map onto $R^{pA}(k_T,y)$ of Eq. (72), which would approach 1 from below for asymptotically high k_T.

At very high energy the geometric scaling regions for the nucleus and the proton will overlap. Namely, the geometric scale for the proton $k^p_{\rm geom}=k_{\rm geom}/A^{1/6}$ will become larger than the saturation scale for the nucleus $Q_s(y)$ allowing for a region of k_T where anomalous dimension sets in for gluon production both in *pA* and *pp*.[2] In this asymptotic region one has to estimate the λ and λ' integrals in Eq. (62) around the saddle point given by Eq. (77) (with Λ instead of Q_{s0} for the λ' integral). Replacing Eq. (71) by the appropriate expression where the saddle points of λ and λ' integrals were given by Eq. (77) with Λ instead of Q_{s0} we obtain the following asymptotic expression at midrapidity ($y=Y/2$):

$$R^{pA}(k_T,y)\big|_{Q_s(y)\le k_T\le k^p_{\rm geom}}\sim A^{-1/6}\exp\left[\frac{\ln^2\frac{k_T}{\Lambda}-\ln^2\frac{k_T}{Q_{s0}}}{14\zeta(3)\bar{\alpha}_s y}\right]. \tag{92}$$

From Eq. (92) we conclude that in the extended geometric scaling region at asymptotically high energies, R^{pA} saturates to a parametrically small lower bound, $R^{pA}\sim A^{-1/6}$, which is independent of energy and is a decreasing function of *A*, or, equivalently, centrality.

To conclude our discussion of high-k_T suppression at the leading twist level we note that, as was recently argued in [65], the running coupling effects in the BFKL evolution may modify the *A*-dependence of the saturation scale given by Eqs. (79) and (83), making $Q_s(y)$ almost independent of *A* at very high energy corresponding to large rapidity *y*. This would result in high-k_T suppression which would not disappear at any k_T. That is $R^{pA}(k_T,y)$ would not approach 1 anymore at high k_T. Instead one would have $R^{pA}(k_T,y)\sim A^{-1/3}$.[3]

C. Next-to-leading twist

Above we have shown that the effect of quantum evolution (49) on the leading twist gluon production cross section in *pA* with $k_T>Q_s(y)$ is to introduce strong suppression of R^{pA}. Here we would like to study the effect of evolution on the gluon production at the next-to-leading twist level. Below we are going to show that if one includes the evolution of Eq. (49) into the next-to-leading twist correction to Eq. (62) it would start contributing towards enhancement of R^{pA} at high k_T. This appears to indicate that multiple rescatterings always tend to enhance gluon production at high k_T. As we will argue later the effect of quantum evolution is much stronger. It dominates at high energies leading to the overall suppression of R^{pA}.

A perturbative solution of Eq. (49) was constructed in [36] giving the forward amplitude of a $q\bar{q}$ dipole scattering on the nucleus as an expansion in powers of $r_T Q_s(y)$

$$N(\boldsymbol{r},\boldsymbol{b},y)=N_1(\boldsymbol{r},\boldsymbol{b},y)+N_2(\boldsymbol{r},\boldsymbol{b},y)+\cdots, \tag{93}$$

where the leading behavior of the *n*th term in the series is $N_n(\boldsymbol{r},\boldsymbol{b},y)\sim[r_T Q_s(y)]^n$. To find the next-to-leading twist correction to the forward scattering amplitude of a *gluon* dipole N_G we substitute Eq. (93) into Eq. (52) obtaining

$$N_G(\boldsymbol{r},\boldsymbol{b},y)=2N_1(\boldsymbol{r},\boldsymbol{b},y)+2N_2(\boldsymbol{r},\boldsymbol{b},y)-[N_1(\boldsymbol{r},\boldsymbol{b},y)]^2+\cdots, \tag{94}$$

where the first term on the right is the leading twist contribution $N_{G1}=2N_1$ given by Eq. (57), and the next two terms shown in Eq. (94) are the next-to-leading twist corrections. Higher twists are not shown in Eq. (94). To calculate the next-to-leading twist correction to gluon forward amplitude

$$\begin{aligned} N_{G2}(\boldsymbol{r},\boldsymbol{b},y)&=2N_2(\boldsymbol{r},\boldsymbol{b},y)-[N_1(\boldsymbol{r},\boldsymbol{b},y)]^2\\ &=2N_2(\boldsymbol{r},\boldsymbol{b},y)-\frac{1}{4}[N_{G1}(\boldsymbol{r},\boldsymbol{b},y)]^2 \end{aligned} \tag{95}$$

we use N_{G1} from Eq. (57) and N_2 calculated in [36]. Employing Eq. (23) from [36] in Eq. (9a) from the same reference would give us the first term on the right-hand side of Eq. (95). In the end we write for a cylindrical nucleus

$$\begin{aligned} N_{G2}(\boldsymbol{r},y)=&-\frac{1}{4}\int\frac{d\lambda_1 d\lambda_2}{(2\pi i)^2}C^A_{\lambda_1}C^A_{\lambda_2}(r_T Q_{s0})^{\lambda_1+\lambda_2}e^{2\bar{\alpha}_s y[\chi(\lambda_1)+\chi(\lambda_2)]}\\ &\times\left(2^{(\lambda_1+\lambda_2)/2}\frac{\Gamma\left(\frac{\lambda_1}{2}\right)\Gamma\left(\frac{\lambda_2}{2}\right)\Gamma\left(1-\frac{\lambda_1+\lambda_2}{2}\right)}{\Gamma\left(1-\frac{\lambda_1}{2}\right)\Gamma\left(1-\frac{\lambda_2}{2}\right)\Gamma\left(\frac{\lambda_1+\lambda_2}{2}\right)}\frac{1}{2[\chi(\lambda_1)+\chi(\lambda_2)-\chi(\lambda_1+\lambda_2)]}+1\right). \end{aligned} \tag{96}$$

[2]The onset of anomalous dimension does not imply saturation and is still a leading twist effect. Therefore Eq. (56) in which *no* saturation in the proton's wave function was assumed is still valid in this region.

[3]The argument presented in this paragraph is due to Larry McLerran.

The slight difference between the factors in the integrands of Eq. (96) and Eq. (23) of [36] is due to different definitions of the coefficients C_λ^A [cf. Eq. (15) of [36] with our Eq. (57)].

The first term in the parentheses of Eq. (96) corresponds to the first term on the right-hand side of Eq. (95). When we will substitute N_{G2} from Eq. (96) into formula (56) for the cross section, this term would give the contribution illustrated in Fig. 7. It corresponds to the case when the gluon is produced still by the linear evolution with the triple Pomeron vertex inserted below the emitted gluon. The rapidity of the triple Pomeron vertex was integrated over in arriving at Eq. (96), with only the dominant contribution corresponding to the vertex being right next to the emitted gluon left [36]. (As was shown in [42] the diagrams where the triple Pomeron vertex is inserted above the produced gluon cancel in the dipole evolution case considered here [37,35] in agreement with the expectation of the AGK cutting rules [66].) The second term in the parenthesis of Eq. (96) and on the right-hand side of Eq. (95) corresponds to the case where the Pomeron splitting occurs precisely at the rapidity position of the gluon production. The emitted gluon is produced by the first step of the nonlinear evolution. (This term is the main difference between the results of [42] and [43].) As can be seen in the estimates performed below, this term contributes 50–100 % of the answer depending on the k_T region in question.

Substituting Eq. (96) in Eq. (56) and integrating over $\boldsymbol{z}$ yields the following contribution to the gluon production cross section at the subleading twist level:

$$\left.\frac{d\sigma^{pA}}{d^2k\,dy}\right|_{\rm SLT} = -\frac{C_F S_p S_A}{\alpha_s 2(2\pi)^3}\int \frac{d\lambda_1 d\lambda_2 d\lambda'}{(2\pi i)^3} C^A_{\lambda_1} C^A_{\lambda_2} C^p_{\lambda'} \left(\frac{Q_{s0}}{k_T}\right)^{\lambda_1+\lambda_2}\left(\frac{\Lambda}{k_T}\right)^{\lambda'}$$
$$\times e^{2\bar{\alpha}_s y[\chi(\lambda_1)+\chi(\lambda_2)]+2\bar{\alpha}_s(Y-y)\chi(\lambda')} 2^{\lambda_1+\lambda_2+\lambda'-3}\frac{\Gamma\left(\frac{\lambda_1+\lambda_2+\lambda'}{2}-1\right)}{\Gamma\left(2-\frac{\lambda_1+\lambda_2+\lambda'}{2}\right)}(\lambda_1+\lambda_2)^2\lambda'^2$$
$$\times\left(2^{(\lambda_1+\lambda_2)/2}\frac{\Gamma\left(\frac{\lambda_1}{2}\right)\Gamma\left(\frac{\lambda_2}{2}\right)\Gamma\left(1-\frac{\lambda_1+\lambda_2}{2}\right)}{\Gamma\left(1-\frac{\lambda_1}{2}\right)\Gamma\left(1-\frac{\lambda_2}{2}\right)\Gamma\left(\frac{\lambda_1+\lambda_2}{2}\right)}\frac{1}{2[\chi(\lambda_1)+\chi(\lambda_2)-\chi(\lambda_1+\lambda_2)]}+1\right). \quad (97)$$

To study the onset of higher twist effects, we are interested in the next-to-leading twist contribution (97) in the region of transverse momenta $k_T \gtrsim k_{\rm geom}$. Performing λ_1 and λ_2 integrations in Eq. (97) around the saddle point (64) and performing the λ' integral in Eq. (97) around the saddle point (65) yields

$$\left.\frac{d\sigma^{pA(2)}}{d^2k\,dy}\right|_{\rm DLA} \approx \frac{C_F S_p S_A\sqrt{\pi}}{\alpha_s(2\pi)^5}\frac{Q_{s0}^4\Lambda^2}{\boldsymbol{k}^6}\frac{\ln^{1/4}\frac{k_T}{\Lambda}\ln^{1/2}\frac{k_T}{Q_{s0}}}{(2\bar{\alpha}_s y)^{3/2}[2\bar{\alpha}_s(Y-y)]^{3/4}}$$
$$\times\left(2\sqrt{\frac{2\bar{\alpha}_s y}{\ln\frac{k_T}{Q_{s0}}}}+\sqrt{\frac{2\bar{\alpha}_s(Y-y)}{\ln\frac{k_T}{\Lambda}}}\right)\exp\left[4\sqrt{2\bar{\alpha}_s y\ln\frac{k_T}{Q_{s0}}}+2\sqrt{2\bar{\alpha}_s(Y-y)\ln\frac{k_T}{\Lambda}}\right]. \quad (98)$$

As one can see from Eq. (98) the next-to-leading twist correction tends to increase gluon production cross section at high k_T. In the region of k_T where Eq. (98) applies, $k_T \gtrsim k_{\rm geom}$, the higher twist corrections are parametrically small and cannot change the leading twist suppression of Eq. (74).

To study higher twist effects in the extended geometric scaling region, $Q_s(y) \lesssim k_T \lesssim k_{\rm geom}$, we evaluate λ_1 and λ_2 integrals in Eq. (97) around the saddle point (77) and do the λ' integral around the saddle point (65) obtaining

$$\left.\frac{d\sigma^{pA(2)}}{d^2k\,dy}\right|_{\rm LLA} \approx \frac{2C_F S_p S_A\sqrt{\pi}}{\alpha_s(2\pi)^5}\frac{Q_{s0}^2\Lambda^2}{\boldsymbol{k}^4}\frac{(C_1^A)^2}{7\zeta(3)}\frac{\ln^{1/4}\frac{k_T}{\Lambda}}{\bar{\alpha}_s y[2\bar{\alpha}_s(Y-y)]^{3/4}}$$
$$\times\left(\sqrt{\frac{2\bar{\alpha}_s(Y-y)}{\ln\frac{k_T}{\Lambda}}}-\frac{2\ln\frac{k_T}{Q_{s0}}}{7\zeta(3)\bar{\alpha}_s y}\right)\exp\left[2(\alpha_P-1)y+2\sqrt{2\bar{\alpha}_s(Y-y)\ln\frac{k_T}{\Lambda}}-\frac{2\ln^2\frac{k_T}{Q_{s0}}}{14\zeta(3)\bar{\alpha}_s y}\right]. \quad (99)$$

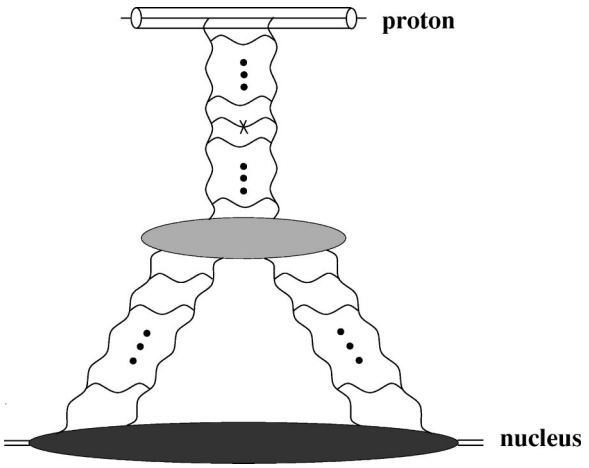

FIG. 7. Gluon production in *pA* collisions at the next-to-leading twist level (see text). The blob in the center indicates a triple Pomeron vertex.

The sign of Eq. (99) is determined by the sign of the expression in the parenthesis. One can see that for very large k_T the expression in the parenthesis can become negative making the overall contribution to the cross section negative. However, Eq. (99) is valid only for $k_T \lesssim k_{\rm geom}$ and, therefore, cannot be used at arbitrary high transverse momenta. At lower k_T the sign changes and the term in Eq. (99) begins to contribute toward enhancement of R^{pA}. The value of k_T at which the sign transition takes place depends on the rapidity in question as well as on the atomic number A of the nucleus. To estimate the transition value of k_T one has to equate two terms in the parenthesis of Eq. (99). Assuming that $\ln k_T/Q_{s0} \gg \ln Q_{s0}/\Lambda$ we obtain

$$k_0 \approx k_{\rm geom}\left(\frac{\Lambda}{Q_{s0}}\right)^{1/3}, \tag{100}$$

with $k_{\rm geom}$ given by Eq. (81). Therefore the transition from suppression to enhancement in Eq. (99) happens at k_0 which is smaller than $k_{\rm geom}$ only by a factor of $A^{-1/18}$, which indicates that the term in Eq. (99) is positive inside most of the extended geometric scaling region contributing to enhancement of gluon production. Here again one should note that Eq. (99) gives us a subleading twist contribution which is parametrically smaller than the leading twist term from Eq. (86) in the k_T region at hand $[Q_s(y) \lesssim k_T \lesssim k_{\rm geom}]$. Equation (99) is thus unlikely to affect the suppression of R^{pA} observed at the leading twist level in Eqs. (91) and (92).

We conclude by observing that even after inclusion of quantum evolution (49) in the gluon production cross section, multiple rescatterings (higher twists) still tend to enhance gluon production at high k_T. In the k_T region considered above, $k_T > Q_s(y)$, these higher twist effects are still parametrically small. In the next section we are going to study the region of k_T where all twists become important, $k_T \sim Q_s(y)$. We will show that the combined effect of all twists is to introduce suppression of the Cronin maximum.

D. Flattening of the Cronin peak

We have demonstrated that the effect of quantum evolution (49) is to introduce suppression of $R^{pA}(k_T,y)$ for $k_T \gtrsim Q_s(y)$ at the leading twist level. Let us now study what happens to $R^{pA}(k_T,y)$ at $k_T \simeq Q_s(y)$ as a result of evolution in energy. We showed in Sec. II that in the quasi-classical approximation the Cronin maximum of the ratio $R^{pA}(\boldsymbol{k},y)$ occurs at $k_T \simeq Q_{s0}$. In this section we will follow the value of the ratio $R^{pA}(k_T = Q_s,y)$ to higher energies when quantum evolution is important. Since the position of the Cronin maximum is likely to be at $k_T \simeq Q_s(y)$ even when evolution is included, by studying $R^{pA}(k_T = Q_s,y)$ we are going to study the dependence of the height of the Cronin maximum on energy or rapidity.

The fact that the scattering amplitude is a constant at the saturation scale [63,56,64] makes our calculation pretty straightforward. First we assume that Mellin transform of the gluon dipole amplitude obtained from the *exact* solution to the evolution equation Eq. (49) via Eq. (52) can be written as

$$N_G(\boldsymbol{z},y) = \int \frac{d\lambda}{2\pi i} \begin{cases} \tilde{C}_\lambda^A [z_T Q_s(y)]^\lambda, & z_T > \dfrac{1}{k_{\rm geom}} \\ C_\lambda^A (z_T Q_{s0})^\lambda e^{2\bar{\alpha}_s \chi(\lambda) y}, & z_T < \dfrac{1}{k_{\rm geom}}. \end{cases} \tag{101}$$

The form of the solution presented in Eq. (101) assumes geometric scaling of N_G down to $z_T \simeq 1/k_{\rm geom}$ and a leading twist expression for smaller z_T in agreement with the analyses of [45,64]. Throughout this section we will use the definition of the saturation scale $Q_s(y)$ from Eq. (79) and the definition of $k_{\rm geom}$ from Eq. (78). Our physical conclusions will be independent of the choice of definitions for saturation and geometric scales.

Note that all information about the nonlinear evolution (49) is encoded in the function $\tilde{C}_\lambda^A$ in Eq. (101). Using Eq. (101) in Eq. (56) we can calculate the differential *pA* gluon production cross section at $k_T = Q_s(y)$. Since $k_{\rm geom}(y) \gg Q_s(y)$ for large y we can set $k_{\rm geom} \to \infty$ neglecting the $z_T < 1/k_{\rm geom}$ part of the integral in Eq. (56). This approximation is justified in the Appendix. We also assume that the dipole amplitude on a proton n_G is still given by the leading twist expression (60) around $k_T \simeq Q_s(y)$, which is a good approximation for a reasonable size nucleus. Substituting the first line of Eqs. (101) and (60) into Eq. (56) we have

$$\left.\frac{d\sigma^{pA}}{d^2k\,dy}\right|_{k_T = Q_s(y)} = \frac{C_F S_p S_A \Lambda^2}{\alpha_s \pi (2\pi)^2} \int_0^\infty dz_T z_T J_0[Q_s(y) z_T] \times \int \frac{d\lambda}{2\pi i} \frac{d\lambda'}{2\pi i} C_{\lambda'}^p \tilde{C}_\lambda^A \lambda^2 \lambda'^2 (z_T \Lambda)^{\lambda'-2} \times [z_T Q_s(y)]^{\lambda-2} e^{2\bar{\alpha}_s (Y-y)\chi(\lambda')}. \tag{102}$$

Performing the z_T integration in Eq. (102) yields

$$\left.\frac{d\sigma^{pA}}{d^2k dy}\right|_{k_T=Q_s(y)} = \frac{C_F S_p S_A}{\alpha_s \pi (2\pi)^2}\int \frac{d\lambda}{2\pi i}\frac{d\lambda'}{2\pi i} \times C_{\lambda'}^{p}\widetilde{C}_{\lambda}^{A}\lambda^2\lambda'^2 2^{\lambda+\lambda'-3}\frac{\Gamma\left(\frac{\lambda+\lambda'}{2}-1\right)}{\Gamma\left(2-\frac{\lambda+\lambda'}{2}\right)} \times\left(\frac{\Lambda}{Q_s(y)}\right)^{\lambda'} e^{2\bar{\alpha}_s(Y-y)\chi(\lambda')}. \tag{103}$$

It can be seen that all energy/rapidity and almost all atomic number dependence in Eq. (103) is given by the λ' integral. Since $Q_s(y)\gg\Lambda$, the integral over λ' in Eq. (103) can be evaluated in the double logarithmic approximation around the saddle point of Eq. (65) taken at $k_T=Q_s(y)$. After that the integral over λ carries almost no dynamical information. The result reads

$$\left.\frac{d\sigma^{pA}}{d^2k dy}\right|_{k_T=Q_s(y)} = \frac{C_F S_p S_A}{\alpha_s (2\pi)^4}\sqrt{\pi}\mathcal{C}_A\frac{\ln^{1/4}\frac{Q_s(y)}{\Lambda}}{[2\bar{\alpha}_s(Y-y)]^{3/4}}\frac{\Lambda^2}{Q_s^2(y)} \times\exp\left(2\sqrt{2\bar{\alpha}_s(Y-y)\ln\frac{Q_s(y)}{\Lambda}}\right), \tag{104}$$

where the integration over λ gave an unknown function $\mathcal{C}_A$ defined as

$$\mathcal{C}_A = \int\frac{d\lambda}{2\pi i}\lambda^2\widetilde{C}_{\lambda}^{A}2^{\lambda}\frac{\Gamma\left(\frac{\lambda}{2}\right)}{\Gamma\left(1-\frac{\lambda}{2}\right)}. \tag{105}$$

Here we assume that $\mathcal{C}_A$ is only weakly (at most logarithmically) dependent on A, as is true for other coefficients like the one shown in Eq. (88). In case of an ''ideal'' geometric scaling the coefficient C_{λ}^{A} in Eq. (101) would be completely A independent ridding $\mathcal{C}_A$ of all of its A dependence as well.

To construct R^{pA} we take the gluon production cross section in pp from Eq. (71) putting $k_T=Q_s(y)$. Substituting Eqs. (104) and (71) into Eq. (32) we get

$$R^{pA}[Q_s(y),y] = \sqrt{\pi}\mathcal{C}_A(2\bar{\alpha}_s)^{1/4}\frac{y^{3/4}}{\sqrt{y}+\sqrt{Y-y}}\ln^{1/4}\left(\frac{Q_s(y)}{\Lambda}\right) \times\frac{Q_s^2(y)}{Q_{s0}^2}\exp\left(-2\sqrt{2\bar{\alpha}_s y\ln\frac{Q_s(y)}{\Lambda}}\right). \tag{106}$$

The energy and A dependence of Eq. (106) can be found using Eq. (79) and keeping in mind that $Q_{s0}=A^{1/6}\Lambda$. Since the definition of the saturation scale (79) is valid up to logarithmic prefactors, we can drop the prefactors in Eq. (106) leaving only

$$R^{pA}[Q_s(y),y]\propto\frac{Q_s^2(y)}{Q_{s0}^2}\exp\left(-2\sqrt{2\bar{\alpha}_s y\ln\frac{Q_s(y)}{\Lambda}}\right). \tag{107}$$

[If one defines $Q_s(y)$ by taking $N_G[z_T=1/Q_s(y),y]$ in the double logarithmic approximation and requiring that $N_G[z_T=1/Q_s(y),y]=\text{const}$ [56,63,64] the prefactors in Eq. (106) would cancel exactly.] Using Eq. (79) in Eq. (107) yields

$$R^{pA}[Q_s(y),y]\propto\exp\left\{4\bar{\alpha}_s y\left(1-\sqrt{1+\frac{\ln A^{1/6}}{2\bar{\alpha}_s y}}\right)\right\}<1. \tag{108}$$

We observe from Eq. (108) that in the course of quantum evolution the Cronin maximum of the ratio R^{pA} decreases with energy until, at very high energy, it saturates at the lowest value $R^{pA}\sim A^{-1/6}$, which is much less than 1. The height of the Cronin peak is also a decreasing function of collision centrality/atomic number A, as can be seen from Eq. (108).[4]

The applicability of Eq. (108) is restricted by the applicability of Eqs. (71) and (104). The latter two equations are valid only in the region where $Q_s(y)$ is larger than the geometric scale of the proton: $Q_s(y)>k_{\text{geom}}/A^{1/6}$ with k_{geom} taken from Eq. (81), since this is where the transition between the saddle points takes place. With the help of Eq. (78) this condition becomes $Q_s(y)<A^{1/6}Q_{s0}$. In the kinematic region of extremely high y where this condition is not satisfied anymore, one has to replace Eqs. (104) and (71) by appropriate cross sections evaluated around the saddle point of Eq. (77). To generalize the conclusions presented above to arbitrary high rapidity let us follow Mueller and Triantafyllopoulos [64] and define the saturation scale by requiring that the power of the exponent in the leading twist expression for N_G given by [cf. Eq. (57)]

$$N_{G1}(\mathbf{z},y) = \int\frac{d\lambda}{2\pi i}C_{\lambda}^{A}e^{2\bar{\alpha}_s\chi(\lambda)y+\lambda\ln(z_T Q_{s0})}$$

is zero and stationary (its derivative with respect to λ is zero) at $z_T=1/Q_s(y)$. These conditions are satisfied at $\lambda_0=1.255$ [64] [our definition of $\chi(\lambda)$ is different from the one used in [64]]. Resulting saturation scale is given by Eq. (83). Arguing that the λ integral in Eq. (57) is dominated by the saddle point in the exponent we conclude that at $z_T=1/Q_s(y)$ the gluon dipole amplitude $N_G[z_T=1/Q_s(y),y]$ is approximately constant at large y [64]

[4]We have recently learned that a similar conclusion regarding centrality dependence of the Cronin peak has been reached by Mueller and collaborators.

$$\int \frac{d\lambda}{2\pi i} C_\lambda^A \left(\frac{Q_{s0}}{Q_s(y)}\right)^\lambda e^{2\bar{\alpha}_s \chi(\lambda) y} = \int \frac{d\lambda}{2\pi i} C_\lambda^A e^{2\bar{\alpha}_s \chi(\lambda) y + \lambda \ln[Q_{s0}/Q_s(y)]} \simeq \text{const}(y, A). \tag{109}$$

Making a similar assumption about the λ' integral in Eq. (103) taken at midrapidity ($y = Y/2$) and remembering that $Q_{s0} = A^{1/6}\Lambda$ yields

$$\left.\frac{d\sigma^{pA}}{d^2k\,dy}\right|_{k_T = Q_s(y), y = Y/2} \sim S_A A^{-\lambda_0/6} \sim A^{2/3 - \lambda_0/6}. \tag{110}$$

Modifying Eq. (62) to give gluon production in pp at $k_T = Q_s(y)$ also taken at midrapidity we obtain

$$\left.\frac{d\sigma^{pp}}{d^2k\,dy}\right|_{k_T = Q_s(y), y = Y/2} = \frac{C_F S_p^2}{4\alpha_s (2\pi)^3} \int \frac{d\lambda}{2\pi i} \frac{d\lambda'}{2\pi i} \lambda^2 \lambda'^2 \times C_\lambda^p C_{\lambda'}^p 2^{\lambda + \lambda'} \frac{\Gamma\left(-1 + \frac{\lambda + \lambda'}{2}\right)}{\Gamma\left(2 - \frac{\lambda + \lambda'}{2}\right)} \times \left(\frac{\Lambda}{Q_s(y)}\right)^{\lambda + \lambda'} e^{2\bar{\alpha}_s [\chi(\lambda) + \chi(\lambda')] y}. \tag{111}$$

Again the λ and λ' integrals in Eq. (111) are dominated by the saddle points at λ_0 giving an energy-independent cross section scaling as

$$\left.\frac{d\sigma^{pp}}{d^2k\,dy}\right|_{k_T = Q_s(y), y = Y/2} \sim A^{-2\lambda_0/6} \tag{112}$$

with atomic number A. Combining Eqs. (110) and (112) with Eq. (32) yields

$$R^{pA}[Q_s(y), y] \propto A^{-1/3 + \lambda_0/6} \text{const}(y) \sim A^{-0.124}, \tag{113}$$

for $\lambda_0 = 1.255$. Note that the power of A in Eq. (113) is pretty close to that following from Eq. (108) and the two powers would be identical for $\lambda_0 = 1$. Note also that taking the expression for R^{pA} in the geometric scaling region from Eq. (92) and extrapolating it down to $k_T = Q_s(y)$ one would obtain a power of A very close to that in Eq. (113) if one uses $Q_s(y)$ from Eq. (79). This conclusion not only verifies the self-consistency of our analysis, but also demonstrates that at asymptotic energies the height of the Cronin maximum becomes (parametrically) equal to the height of the rest of the R^{pA} curve in the extended geometric scaling region. This is likely to indicate that at these energies the curve flattens out and the Cronin peak disappears.

With the help of Eq. (113) we conclude that at high rapidities or energies the Cronin maximum decreases with energy and centrality, with $R^{pA}[Q_s(y), y]$ becoming less than 1. Eventually, at very high energy, the Cronin peak flattens out and saturates to an energy independent lower limit given by Eq. (113), which is parametrically suppressed by powers of A.

E. Suppression deep inside the saturation region

Above we have shown that nonlinear evolution (49) introduces suppression of gluon production in pA collisions making $R^{pA} < 1$ for $k_T \gtrsim Q_s(y)$. In the region of smaller k_T, $k_T \ll Q_s(y)$, we observed in Sec. III B that in the quasi-classical case of the McLerran-Venugopalan model the ratio $R^{pA} \ll 1$ [see Eq. (47)]. When the quantum evolution (49) is included it makes sense to consider the interval of low k_T bounded from below by the saturation scale of the proton $\Lambda_s(y)$, such that $\Lambda_s(y) \ll k_T \ll Q_s(y)$. [For $k_T \lesssim \Lambda_s(y)$ the proton wave function also saturates and particle production in both pp and pA becomes similar to the case of AA, which has not been resolved even at the quasi-classical level [22,23,33]. Inclusion of evolution in AA is an even more difficult problem which we are not going to address here.] If k_T is larger than the geometric scale of the proton $k_{\text{geom}}/A^{1/6}$ [but still much less than $Q_s(y)$] we can use Eq. (71) to describe the gluon production cross section in pp. Deep inside the saturation region in pA the gluon production has been estimated in [42]. Employing Eq. (57) from [42] together with Eq. (71) we conclude that at midrapidity

$$R^{pA}[k_{\text{geom}}^p < k_T \ll Q_s(y), y] \sim \frac{k_T^2}{Q_{s0}^2} e^{-2\sqrt{2\alpha_s y \ln k_T/\Lambda}}. \tag{114}$$

Equation (114) shows that inclusion of quantum evolution only introduces more suppression into R^{pA} at $k_T \ll Q_s(y)$, making it a decreasing function of both the atomic number and energy. At very high energy k_T may become smaller than the geometric scale for the proton $k_{\text{geom}}/A^{1/6}$ and the gluon production in pp would be driven by the saddle point (77) with Λ instead of Q_{s0}. Similarly to how it was done in [42] for DLA, one can estimate the gluon production cross section (56) deep inside the saturation region with the dipole amplitude on the proton evaluated around the LLA saddle point $\lambda' \approx 1$. The result at midrapidity yields

$$R^{pA}[\Lambda_s(y) \ll k_T \lesssim k_{\text{geom}}^p] \sim A^{-1/3} \frac{Q_s(y)}{\Lambda} \exp\left[-(\alpha_P - 1) y + \frac{2\ln^2(k_T/\Lambda) - \ln^2[Q_s(y)/\Lambda]}{14\zeta(3)\bar{\alpha}_s y}\right]. \tag{115}$$

Therefore at very high energies the ratio R^{pA} becomes almost independent of k_T even at very low k_T. Using the saturation scale from Eq. (79) in Eq. (115) at asymptotic energies gives

$$R^{pA}[\Lambda_s(y) \ll k_T \lesssim k_{\text{geom}}^p] \sim A^{-0.2} e^{-1.0\bar{\alpha}_s y}. \tag{116}$$

We observe again that nonlinear evolution leaves R^{pA} very small at $k_T \ll Q_s(y)$. R^{pA} given by Eq. (116) is a decreasing function of both rapidity or energy and centrality. This conclusion seems natural, since the saturation effects are known to soften the low-k_T gluon spectra in pA compared to pp.

F. Toy model

To illustrate the conclusions reached above let us construct a simple toy model exhibiting suppression of R^{pA} at all k_T. We start with the quasi-classical formula for gluon production in pA in the following form which could be obtained from Eq. (40) for a cylindrical nucleus and for azimuthally symmetric N_G:

$$\frac{d\sigma^{pA}}{d^2k dy} = \frac{\alpha_s C_F}{\pi^2}\frac{S_A}{k_T^2}\int_0^\infty dz_T J_0(k_T z_T)\ln\frac{1}{z_T\Lambda} \times \partial_{z_T}[z_T \partial_{z_T} N_G(z_T, y=0)]. \tag{117}$$

With the increase of energy the gluon dipole amplitude on the nucleus will reach saturation. Therefore its z_T dependence will change more significantly than for the corresponding amplitude on the proton, which will stay unsaturated. (Of course at very high energy the dipole amplitude on the proton will also reach saturation, but we are not going to consider that energy range here.) Therefore in our toy model we will assume for simplicity that the gluon dipole amplitude on the proton remains unchanged with increasing energy, giving $\ln 1/(z_T\Lambda)$ in Eq. (117). We will model the gluon dipole amplitude at high energy by a Glauber-like unitary expression

$$N_G^{\text{toy}}(z_T, y) = 1 - e^{-z_T Q_s(y)}, \tag{118}$$

which mimics the onset of anomalous dimension $\lambda = 1$ by the linear term in the exponent. The saturation scale $Q_s(y)$ in Eq. (118) is some increasing function of y which can be taken from Eq. (79) or from Eq. (83). Indeed the amplitude in Eq. (118) has an incorrect small-z_T behavior, scaling proportionally to z_T instead of z_T^2 as shown in Eq. (14). If Eq. (118) is used in Eq. (117) it would lead to an incorrect high-k_T behavior of the resulting cross section. We therefore argue that Eq. (118) is, probably, a reasonable model for N_G inside the saturation and extended geometric scaling regions ($1/z_T \sim k_T < k_{\text{geom}}$), but should not be used for very small z_T/high k_T ($1/z_T \sim k_T > k_{\text{geom}}$).

Substituting Eq. (118) into Eq. (117) and integrating over z_T yields

$$\frac{d\sigma^{pA}_{\text{toy}}}{d^2k dy} = \frac{\alpha_s C_F}{\pi^2}\frac{S_A}{k_T^2}\frac{Q_s}{k_T^2+Q_s^2}\Bigg[-Q_s(k_T^2+Q_s^2) + \sqrt{k_T^2+Q_s^2}\Bigg(2Q_s^2 + \gamma k_T^2 + k_T^2 \ln\frac{2(k_T^2+Q_s^2)}{k_T\Lambda} + \frac{k_T^2}{2}\ln\frac{\sqrt{k_T^2+Q_s^2}-Q_s}{\sqrt{k_T^2+Q_s^2}+Q_s}\Bigg)\Bigg], \tag{119}$$

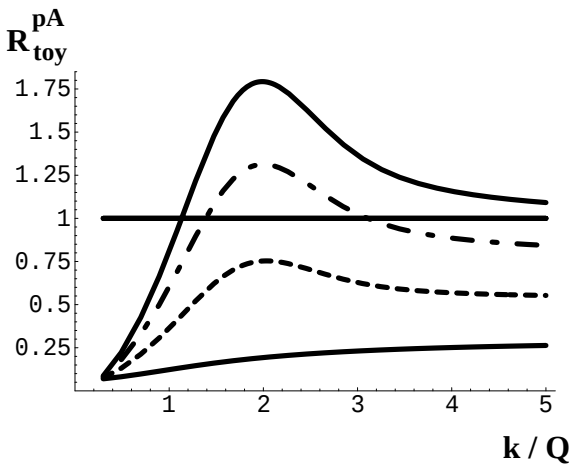

FIG. 8. The ratio R^{pA} plotted as a function of k_T/Q_s for (i) the McLerran-Venugopalan model, which is valid for moderate energies (upper solid line); (ii) our toy model for very high energies/rapidities from Eq. (121) (lower solid line); and (iii) an interpolation to intermediate energies (dash-dotted and dashed lines). The cutoff is $\Lambda = 0.3Q_s$.

where γ is the Euler's constant and $Q_s = Q_s(y)$. The corresponding gluon production cross section for pp is obtained by expanding Eq. (119) to the lowest order at high k_T and substituting Λ instead of Q_s and S_p instead of S_A:

$$\frac{d\sigma^{pp}_{\text{toy}}}{d^2k dy} = \frac{\alpha_s C_F}{\pi^2}\frac{S_p \Lambda}{k_T^3}\left(\ln\frac{2k_T}{\Lambda} + \gamma\right). \tag{120}$$

Of course in Eq. (120) one implicitly assumes that anomalous dimension has set in for only one of the protons in pp. This assumption is not valid at midrapidity, but may be used to study particle production at rapidities near the fragmentation region of one of the protons.

Substituting Eqs. (119) and (120) in Eq. (32) yields

$$R^{pA}_{\text{toy}}(k_T, y) = \frac{k_T\Lambda}{Q_s(k_T^2+Q_s^2)[\ln(2k_T/\Lambda)+\gamma]}\Bigg[-Q_s(k_T^2+Q_s^2) + \sqrt{k_T^2+Q_s^2}\Bigg(2Q_s^2 + \gamma k_T^2 + k_T^2\ln\frac{2(k_T^2+Q_s^2)}{k_T\Lambda} + \frac{k_T^2}{2}\ln\frac{\sqrt{k_T^2+Q_s^2}-Q_s}{\sqrt{k_T^2+Q_s^2}+Q_s}\Bigg)\Bigg], \tag{121}$$

in which we assumed that Λ is the saturation scale of the proton such that $Q_s^2 = A^{1/3}\Lambda^2$ even at high energy.

The toy model $R^{pA}_{\text{toy}}(k_T, y)$ from Eq. (121) is plotted as a function of k_T/Q_s in Fig. 8 for $\Lambda = 0.3Q_s$ (lower solid curve). It exhibits suppression of gluon production in pA at all values of k_T leveling off at $R^{pA}_{\text{toy}} \sim \Lambda/Q_s \sim A^{-1/6}$ for $k_T \gtrsim Q_s$ at high energy, in agreement with our conclusions of Secs. III B and III D.

Our toy model (121) represents the high energy asymptotics of R^{pA}. To compare it to lower energies, we also plot

R^{pA} for the quasi-classical McLerran-Venugopalan model given by Eq. (34) (upper solid curve in Fig. 8). As the energy increases the upper solid line in Fig. 8 would decrease eventually turning into the lower solid line. The corresponding intermediate energy stages are shown by the dash-dotted and dashed lines in Fig. 8. These lines are for illustrative purposes only and do not correspond to any toy model. They demonstrate how the Cronin peak gradually disappears as energy or rapidity increase.

V. CONCLUSIONS

In this paper we have demonstrated that saturation effects in the gluon production in *pA* at moderate energy can be taken into account in the quasi-classical framework of the McLerran-Venugopalan model, which includes Glauber-Mueller multiple rescatterings, resulting only in Cronin enhancement of produced gluons at $k_T=(1-2)Q_{s0}$, as was shown in Fig. 4 and in Eq. (37). Similar conclusions have been reached in [48]. In this quasi-classical approximation the height and position of the Cronin peak are increasing functions of centrality as indicated by Eq. (38).

We have also shown that at higher energies or rapidities, when quantum evolution becomes important, it introduces suppression of gluons produced in *pA* collisions at all values of k_T, as compared to the number of gluons produced in *pp* collisions scaled up by the number of collisions $N_{\rm coll}$, as suggested previously [8]. The resulting R^{pA} at high energy or rapidity is a decreasing function of centrality. We have considered three different complimentary regions of k_T, which cover together all of the k_T range

(i) $k_T>Q_s(y)$ region. Gluon production cross section in *pA* is dominated by the leading twist effects in this region of k_T. We have shown how the leading twist suppression arises in the double logarithmic approximation for $k_T>k_{\rm geom}\gg Q_s(y)$ with the corresponding $R^{pA}(k_T,y)$ given by Eq. (72), which approaches 1 as $k_T\to\infty$. At $Q_s(y)<k_T\lesssim k_{\rm geom}$ the leading twist suppression is mainly due to the change in anomalous dimension λ from its double logarithmic value (64) to the leading logarithmic value (77). $R^{pA}(k_T,y)$ for this k_T window is given by Eq. (89) leading to suppression described by Eq. (91). At very high energies, when the extended geometric scaling regions of the proton and the nucleus overlap [for $Q_s(y)<k_T\lesssim k^p_{\rm geom}$] the decrease of R^{pA} with energy stops at roughly $R^{pA}\sim A^{-1/6}$ as follows from Eq. (92). This leading twist effect has been originally pointed out in [8]. We have not considered suppression mechanisms that may stem from running of the coupling constant, which would modify the *A* dependence of the saturation scale [65].

(ii) $k_T\sim Q_s(y)$ is the position of the Cronin maximum in the quasi-classical approximation. We began the analysis of this k_T region by studying higher twists in the adjacent region of $k_T>Q_s(y)$. The next-to-leading twist term was shown to contribute towards enhancement of R^{pA} at high-k_T even when evolution is included. However, higher twist effects are parametrically small at $k_T>Q_s(y)$ and cannot change our leading twist conclusions about suppression. To assess the contribution of all twists we studied the behavior of the Cronin maximum $[k_T\sim Q_s(y)]$ with increasing energy. We showed that R^{pA} at $k_T=Q_s(y)$ is a decreasing function of energy or rapidity and centrality saturating at the energy-independent lower bound given by Eq. (113). Since the height of the Cronin maximum becomes parametrically of the same order as the rest of R^{pA} at higher k_T given by Eq. (92), we conclude that the Cronin peak disappears at asymptotically high energies or rapidities.

(iii) $k_T\ll Q_s(y)$ region. The suppression of R^{pA} deep inside the saturation region, $k_T\ll Q_s(y)$, only gets stronger as the evolution (49) is included [see Eq. (116)].

Our results are summarized in Fig. 8.

It is interesting to observe that the behavior of R^{pA} at high energies is qualitatively different from what one would expect by taking the quasi-classical expression (34) and letting Q_s in it increase with energy. In the case of DIS a similar trick where one replaces Q_{s0} in the Glauber-Mueller expression for the dipole cross section (9) by the energy dependent Q_s from, for instance, Eq. (79) leads to correct qualitative behavior of resulting F_2 structure function and even generates some successful phenomenology [67]. However, as we showed above, a naive generalization of the McLerran-Venugopalan model by increasing Q_s with energy does not work for R^{pA} even at the qualitative level.

The analysis in the paper was, of course, done for sufficiently high energy and/or rapidity, such that the saturation approach was assumed to be still valid for the highest k_T involved. This implies that the effective Bjorken *x* is still sufficiently small for all k_T we consider. The extent to which this treatment applies at high k_T hadron production at RHIC is difficult to assess theoretically. We thus eagerly await the results of the experimental analyses of centrality dependence of hadron production above the Cronin region ($k_T\geqslant 6$ GeV). It is also very important to extend the present measurements away from the central rapidity region to separate initial state effects from possible energy loss in cold nuclear matter. Indeed, in the deuteron fragmentation region, the effects of saturation in the Au wave function will be enhanced, while the density of the produced particles (see, e.g., the predictions in [68]) and thus the associated energy loss will be minimal. In the Au fragmentation region the opposite will be true.

We therefore conclude that if the effects of quantum evolution and anomalous dimension are observed in the forward rapidity region of *d*-Au collisions at RHIC, they would manifest themselves by reducing R^{dA} at all k_T as shown in Fig. 8, eliminating the Cronin enhancement. R^{dA} will become a *decreasing* function of centrality. The *pA* program at LHC would observe an even stronger suppression of R^{pA}. However, it might be that the quantum evolution effects are still not important even in the forward region of *d*-Au collisions at RHIC. Then reduction of R^{dA} going from the midrapidity to deuteron fragmentation region should be rather mild and the Cronin peak would not disappear in the forward region. The relevant particle production physics would be described by the McLerran-Venugopalan model. The height of the Cronin peak would then be an *increasing* function of centrality.

If the forthcoming data on R^{dA} in the forward rapidity region of *d*-Au collisions would have no high-p_T suppression and would exhibit only a strong Cronin maximum which is

an increasing function of centrality in agreement with predictions of multiple rescattering models described in Sec. III [48,49,51–54], then all of the observed high-p_T suppression in Au-Au collisions would have to be attributed to the final state effects. However, if the future R^{dA} data in the forward rapidity region exhibits suppression either for all p_T or at high p_T with R^{dA} being a decreasing function of centrality as described in this paper (see also [8]), then a fraction of R^{AA} suppression in the forward rapidity region of Au-Au collisions should be attributed to initial state quantum evolution effects. Indeed, there is some evidence [4] that the high k_T suppression in Au-Au collisions increases between the pseudorapidities $\eta=0$ and $\eta=2.2$.

The d-Au data at $y\simeq 0$ [1–4] also suggest suppression of the yields of charged hadrons [3] and neutral pions [1] at $k_T \geqslant 6$ GeV, though the suppression is not significant statistically. If this initial-state effect is confirmed, it should also be taken into account in the interpretation of Au-Au results at $y\simeq 0$.

The d-Au results will thus allow one to clarify the relative importance of initial and final state interactions at different transverse momenta and rapidities of the produced particles. They will be indispensable for establishing a complete physical picture of heavy ion collisions at RHIC energies.

Note added: After the first version of this paper appeared, a similar analysis has been done in [69–71]. The analyses of [69–71] agree with our conclusions on the presence of the Cronin effect in the quasi-classical approximation. The results of [69,71] are also in agreement with our conclusion about high-p_T suppression of *gluon* production.

ACKNOWLEDGMENTS

We are grateful to Al Mueller for illuminating discussions of the earlier version of the paper, Eugene Levin and Larry McLerran for continuing enjoyable collaborations on the subject. The authors would like to thank Alberto Accardi, Rolf Baier, Miklos Gyulassy, Jamal Jalilian-Marian, Alex Kovner, Xin-Nian Wang, Heribert Weigert, and Urs Wiedemann for stimulating and informative discussions. The research of D.K. was supported by the U.S. Department of Energy under Contract No. DE-AC02-98CH10886. The work of Yu.K. was supported in part by the U.S. Department of Energy under Grant No. DE-FG03-97ER41014. The work of K.T. was sponsored in part by the U.S. Department of Energy under Grant No. DE-FG03-00ER41132.

APPENDIX

Here we are going to derive Eq. (102). In writing down Eq. (102) we assumed that the integration region $z_T < 1/k_{\rm geom}$ is negligible. To justify this approximation let us start by substituting Eq. (101) into Eq. (56). We find

$$\left.\frac{d\sigma^{pA}}{d^2k dy}\right|_{k_T=Q_s(y)} = \frac{C_F S_p S_A}{\alpha_s \pi (2\pi)^2 Q_s^2(y)} \left\{ \int_0^{1/k_{\rm geom}} dz_T z_T J_0[Q_s(y) z_T] \int \frac{d\lambda}{2\pi i} \int \frac{d\lambda'}{2\pi i} C_\lambda^p, C_\lambda^A \lambda^2 \lambda'^2 \Lambda^2 Q_{s0}^2 (z_T \Lambda)^{\lambda'-2} (z_T Q_{s0})^{\lambda-2} \right.$$
$$\times e^{2\bar{\alpha}_s y \chi(\lambda) + 2\bar{\alpha}_s (Y-y)\chi(\lambda')} + \int_{1/k_{\rm geom}}^{\infty} dz_T z_T J_0[Q_s(y) z_T] \int \frac{d\lambda}{2\pi i} \int \frac{d\lambda'}{2\pi i} C_\lambda^p, \tilde{C}_\lambda^A \lambda^2 \lambda'^2 \Lambda^2 Q_s^2(y)$$
$$\left. \times (z_T \Lambda)^{\lambda'-2} [z_T Q_s(y)]^{\lambda-2} e^{2\bar{\alpha}_s (Y-y)\chi(\lambda')} \right\}. \tag{A1}$$

The difference between Eq. (A1) and the target Eq. (102) is

$$\frac{C_F S_p S_A}{\alpha_s \pi (2\pi)^2 Q_s^2(y)} \int_0^{1/k_{\rm geom}} dz_T z_T^{-3} J_0[Q_s(y) z_T]$$
$$\times \int \frac{d\lambda}{2\pi i} \int \frac{d\lambda'}{2\pi i} C_\lambda^p, \lambda^2 \lambda'^2 (z_T \Lambda)^{\lambda'} e^{2\bar{\alpha}_s (Y-y)\chi(\lambda')}$$
$$\times [C_\lambda^A (z_T Q_{s0})^\lambda e^{2\bar{\alpha}_s y \chi(\lambda)} - \tilde{C}_\lambda^A [z_T Q_s(y)]^\lambda]. \tag{A2}$$

Since $k_{\rm geom} \gg Q_s(y)$ we can neglect the argument of the Bessel function in the integral in Eq. (A2) putting $J_0(0)=1$. Integration over z_T then yields

$$\frac{C_F S_p S_A}{\alpha_s \pi (2\pi)^2} \int \frac{d\lambda}{2\pi i} \int \frac{d\lambda'}{2\pi i} C_\lambda^p, \lambda^2 \lambda'^2 e^{2\bar{\alpha}_s (Y-y)\chi(\lambda')}$$
$$\times \frac{1}{\lambda+\lambda'-2} \left(\frac{\Lambda}{k_{\rm geom}}\right)^{\lambda'} \frac{k_{\rm geom}^2}{Q_s^2(y)}$$
$$\times \left[C_\lambda^A e^{2\bar{\alpha}_s y \chi(\lambda)} \left(\frac{Q_{s0}}{k_{\rm geom}}\right)^\lambda - \tilde{C}_\lambda^A \left(\frac{Q_s(y)}{k_{\rm geom}}\right)^\lambda \right]. \tag{A3}$$

Due to the inequality $k_{\rm geom} \gg Q_s(y) \gg \Lambda$, the integration over λ' in Eq. (A3) is dominated by the saddle point at $\lambda' \approx 2$, as

shown in Eqs. (63) and (65). The integral over λ in Eq. (A3) becomes

$$\int \frac{d\lambda}{2\pi i} \frac{\lambda^2}{\lambda+\lambda'-2}\left[C_\lambda^A e^{2\bar{\alpha}_s y \chi(y)}\left(\frac{Q_{s0}}{k_{\rm geom}}\right)^\lambda - \tilde{C}_\lambda^A\left(\frac{Q_s(y)}{k_{\rm geom}}\right)^\lambda\right]$$

$$\approx \int \frac{d\lambda}{2\pi i}\lambda\left[C_\lambda^A e^{2\bar{\alpha}_s y \chi(y)}\left(\frac{Q_{s0}}{k_{\rm geom}}\right)^\lambda - \tilde{C}_\lambda^A\left(\frac{Q_s(y)}{k_{\rm geom}}\right)^\lambda\right]$$

$$= -\frac{\partial}{\partial \ln k_{\rm geom}}\{N_G[z_T \to (1/k_{\rm geom})^-, y]$$

$$- N_G[z_T \to (1/k_{\rm geom})^+, y]\} = 0, \tag{A4}$$

where we assumed that $N_G(\boldsymbol{z},y)$ and its derivatives with respect to z_T from Eq. (101) are smooth functions of z_T such that the difference of the above limits is zero. This assumption is justified since $N_G(\boldsymbol{z},y)$ is proportional to the scattering matrix which is an analytic function of its variables. Equation (49) makes $N_G(\boldsymbol{z},y)$ analytic by construction.

We showed that the difference between the exact Eq. (A1) and our Eq. (102) is zero, making the two equations equal, as desired. However, the above proof required that the representation of $N_G(\boldsymbol{z},y)$ given by Eq. (101) has a smooth matching of the two regions at $z_T = 1/k_{\rm geom}$, i.e., that representation (101) is not just a good approximation but an exact identity. To show that no such assumption is required to prove that the expression in Eq. (A3) is a negligible correction to Eq. (102) let us estimate the energy dependence of the first term in Eq. (A3). The second term in Eq. (A3) is negative and can only make the overall contribution smaller. Employing double logarithmic approximation for λ and λ' integrals and using Eqs. (79) and (78) we derive (setting $y = Y/2$ for simplicity)

$$\int \frac{d\lambda}{2\pi i}\int \frac{d\lambda'}{2\pi i} C^p_{\lambda'} \lambda^2 \lambda'^2 e^{2\bar{\alpha}_s (Y-y)\chi(\lambda')} \frac{1}{\lambda+\lambda'-2}$$

$$\times \left(\frac{\Lambda}{k_{\rm geom}}\right)^{\lambda'} \frac{k_{\rm geom}^2}{Q_s^2(y)} C_\lambda^A e^{2\bar{\alpha}_s y \chi(\lambda)}\left(\frac{Q_{s0}}{k_{\rm geom}}\right)^\lambda$$

$$\propto \frac{\Lambda^2 Q_{s0}^2 A^{1/6\sqrt{2}}}{k_{\rm geom}^2 Q_s^2(y)} e^{8\sqrt{2}\bar{\alpha}_s y}$$

$$\propto A^{-1/3+1/(6\sqrt{2})} e^{-4\bar{\alpha}_s y(3-2\sqrt{2})}, \tag{A5}$$

which is a decreasing function of rapidity and centrality. It is obviously negligible compared to the increasing function of y given by Eq. (104). This accomplishes our proof of Eq. (102).

[1] PHENIX Collaboration, S.S. Adler *et al.*, Phys. Rev. Lett. **91**, 072303 (2003).

[2] PHOBOS Collaboration, B.B. Back *et al.*, Phys. Rev. Lett. **91**, 072302 (2003).

[3] STAR Collaboration, J. Adams *et al.*, Phys. Rev. Lett. **91**, 072304 (2003).

[4] BRAHMS Collaboration, I. Arsene *et al.*, Phys. Rev. Lett. **91**, 072305 (2003).

[5] PHENIX Collaboration, K. Adcox *et al.*, Phys. Lett. B **561**, 82 (2003); PHENIX Collaboration, S.S. Adler *et al.*, Phys. Rev. Lett. **91**, 072301 (2003).

[6] PHOBOS Collaboration, B.B. Back *et al.*, nucl-ex/0302015.

[7] STAR Collaboration, J. Adams *et al.*, Phys. Rev. Lett. **91**, 172302 (2003); STAR Collaboration, C. Adler *et al.*, *ibid.* **89**, 202301 (2002).

[8] D. Kharzeev, E. Levin, and L. McLerran, Phys. Lett. B **561**, 93 (2003).

[9] L.V. Gribov, E.M. Levin, and M.G. Ryskin, Phys. Rep. **100**, 1 (1983).

[10] A.H. Mueller and J.w. Qiu, Nucl. Phys. **B268**, 427 (1986).

[11] J.P. Blaizot and A.H. Mueller, Nucl. Phys. **B289**, 847 (1987).

[12] L.D. McLerran and R. Venugopalan, Phys. Rev. D **49**, 2233 (1994); **49**, 3352 (1994); **50**, 2225 (1994).

[13] Y.V. Kovchegov, Phys. Rev. D **54**, 5463 (1996); **55**, 5445 (1997); J. Jalilian-Marian, A. Kovner, L.D. McLerran, and H. Weigert, *ibid.* **55**, 5414 (1997).

[14] J. D. Bjorken, FERMILAB-PUB-82-059-THY (unpublished).

[15] X.N. Wang, M. Gyulassy, and M. Plumer, Phys. Rev. D **51**, 3436 (1995); M. Gyulassy, P. Levai, and I. Vitev, Phys. Rev. Lett. **85**, 5535 (2000); M. Gyulassy, I. Vitev, X.N. Wang, and B.W. Zhang, nucl-th/0302077; M. Gyulassy, I. Vitev, and X.N. Wang, Phys. Rev. Lett. **86**, 2537 (2001); I. Vitev and M. Gyulassy, *ibid.* **89**, 252301 (2002); X.N. Wang, nucl-th/0305010.

[16] R. Baier, Y.L. Dokshitzer, A.H. Mueller, S. Peigne, and D. Schiff, Nucl. Phys. **B483**, 291 (1997); **B484**, 265 (1997); **B478**, 577 (1996); R. Baier, Y.L. Dokshitzer, A.H. Mueller, and D. Schiff, Phys. Rev. C **58**, 1706 (1998); Nucl. Phys. **B531**, 403 (1998); J. High Energy Phys. **09**, 033 (2001); R. Baier, Y.L. Dokshitzer, S. Peigne, and D. Schiff, Phys. Lett. B **345**, 277 (1995).

[17] A. Kovner and U.A. Wiedemann, hep-ph/0304151, and references therein.

[18] D. Kharzeev and M. Nardi, Phys. Lett. B **507**, 121 (2001); D. Kharzeev and E. Levin, *ibid.* **523**, 79 (2001); D. Kharzeev, E. Levin, and M. Nardi, hep-ph/0111315.

[19] J. Schaffner-Bielich, D. Kharzeev, L.D. McLerran, and R. Venugopalan, Nucl. Phys. **A705**, 494 (2002).

[20] Y.V. Kovchegov and K.L. Tuchin, Nucl. Phys. **A708**, 413 (2002); **A717**, 249 (2003).

[21] R. Baier, A.H. Mueller, D. Schiff, and D.T. Son, Phys. Lett. B **539**, 46 (2002).

[22] A. Krasnitz and R. Venugopalan, Phys. Rev. Lett. **84**, 4309 (2000); **86**, 1717 (2001); A. Krasnitz, Y. Nara, and R. Venugopalan, Phys. Rev. Lett. **87**, 192302 (2001); Nucl. Phys. **A727**, 427 (2003).

[23] T. Lappi, Phys. Rev. C **67**, 054903 (2003).

[24] STAR Collaboration, J. Adams *et al.*, nucl-ex/0306007.

[25] PHENIX Collaboration, S.S. Adler *et al.*, hep-ex/0307019.

[26] Y.V. Kovchegov and M. Strikman, Phys. Lett. B **516**, 314 (2001).

[27] E. Gotsman, E. Levin, U. Maor, L.D. McLerran, and K. Tuchin, Nucl. Phys. **A683**, 383 (2001).
[28] B.Z. Kopeliovich, Phys. Rev. C **68**, 044906 (2003).
[29] Yu.V. Kovchegov and A.H. Mueller, Nucl. Phys. **B529**, 451 (1998).
[30] B.Z. Kopeliovich, A.V. Tarasov, and A. Schafer, Phys. Rev. C **59**, 1609 (1999).
[31] A. Dumitru and L.D. McLerran, Nucl. Phys. **A700**, 492 (2002).
[32] A. Kovner and U.A. Wiedemann, Phys. Rev. D **64**, 114002 (2001).
[33] Y.V. Kovchegov, Nucl. Phys. **A692**, 557 (2001).
[34] E.A. Kuraev, L.N. Lipatov, and V.S. Fadin, Sov. Phys. JETP **45**, 199 (1977) [Zh. Eksp. Teor. Fiz. **72**, 377 (1977)]; I.I. Balitsky and L.N. Lipatov, Sov. J. Nucl. Phys. **28**, 822 (1978) [Yad. Fiz. **28**, 1597 (1978)].
[35] Y.V. Kovchegov, Phys. Rev. D **60**, 034008 (1999).
[36] Y.V. Kovchegov, Phys. Rev. D **61**, 074018 (2000).
[37] A.H. Mueller, Nucl. Phys. **B415**, 373 (1994); A.H. Mueller and B. Patel, *ibid.* **B425**, 471 (1994); A.H. Mueller, *ibid.* **B437**, 107 (1995); Z. Chen and A.H. Mueller, *ibid.* **B451**, 579 (1995).
[38] I. Balitsky, Nucl. Phys. **B463**, 99 (1996); hep-ph/9706411; Phys. Rev. D **60**, 014020 (1999).
[39] J. Jalilian-Marian, A. Kovner, A. Leonidov, and H. Weigert, Nucl. Phys. **B504**, 415 (1997); Phys. Rev. D **59**, 014014 (1999); **59**, 034007 (1999); **59**, 099903(E) (1999); J. Jalilian-Marian, A. Kovner, and H. Weigert, *ibid.* **59**, 014015 (1999); A. Kovner, J.G. Milhano, and H. Weigert, *ibid.* **62**, 114005 (2000); H. Weigert, Nucl. Phys. **A703**, 823 (2002).
[40] E. Iancu, A. Leonidov, and L.D. McLerran, Nucl. Phys. **A692**, 583 (2001); Phys. Lett. B **510**, 133 (2001); E. Iancu and L.D. McLerran, *ibid.* **510**, 145 (2001); E. Ferreiro, E. Iancu, A. Leonidov, and L. McLerran, Nucl. Phys. **A703**, 489 (2002).
[41] M. Braun, Eur. Phys. J. C **16**, 337 (2000).
[42] Yu.V. Kovchegov and K. Tuchin, Phys. Rev. D **65**, 074026 (2002).
[43] M.A. Braun, Phys. Lett. B **483**, 105 (2000).
[44] Y.V. Kovchegov, Phys. Rev. D **64**, 114016 (2001).
[45] E. Iancu, K. Itakura, and L. McLerran, Nucl. Phys. **A708**, 327 (2002).
[46] A.H. Mueller, Nucl. Phys. **B335**, 115 (1990).
[47] J.W. Cronin, H.J. Frisch, M.J. Shochet, J.P. Boymond, R. Mermod, P.A. Piroue, and R.L. Sumner, Phys. Rev. D **11**, 3105 (1975).
[48] B.Z. Kopeliovich, J. Nemchik, A. Schafer, and A.V. Tarasov, Phys. Rev. Lett. **88**, 232303 (2002).
[49] A. Accardi and M. Gyulassy, nucl-th/0308029.
[50] M.G. Ryskin, Yad. Fiz. **32**, 259 (1980); E.M. Levin and M.G. Ryskin, *ibid.* **32**, 802 (1980); Nucl. Phys. **B304**, 805 (1988).
[51] X.N. Wang, Phys. Rev. Lett. **81**, 2655 (1998); M. Gyulassy and P. Levai, Phys. Lett. B **442**, 1 (1998); X.N. Wang, Phys. Rev. C **61**, 064910 (2000).
[52] E. Wang and X.N. Wang, Phys. Rev. C **64**, 034901 (2001); Y. Zhang, G. Fai, G. Papp, G.G. Barnafoldi, and P. Levai, *ibid.* **65**, 034903 (2002); I. Vitev and M. Gyulassy, Phys. Rev. Lett. **89**, 252301 (2002).
[53] I. Vitev, Phys. Lett. B **562**, 36 (2003).
[54] X.N. Wang, Phys. Lett. B **565**, 116 (2003); nucl-th/0305010; X. Zhang and G. Fai, hep-ph/0306227; G.G. Barnafoldi, G. Papp, P. Levai, and G. Fai, nucl-th/0307062.
[55] A.M. Stasto, K. Golec-Biernat, and J. Kwiecinski, Phys. Rev. Lett. **86**, 596 (2001).
[56] E. Levin and K. Tuchin, Nucl. Phys. **B573**, 833 (2000).
[57] L. Frankfurt, G.A. Miller, and M. Strikman, Phys. Lett. B **304**, 1 (1993).
[58] F. Gelis and J. Jalilian-Marian, Phys. Rev. D **67**, 074019 (2003); A. Dumitru and J. Jalilian-Marian, Phys. Lett. B **547**, 15 (2002); Phys. Rev. Lett. **89**, 022301 (2002).
[59] M. Anselmino, E. Predazzi, S. Ekelin, S. Fredriksson, and D.B. Lichtenberg, Rev. Mod. Phys. **65**, 1199 (1993).
[60] V. Del Duca, M.E. Peskin, and W.K. Tang, Phys. Lett. B **306**, 151 (1993).
[61] K.J. Eskola, A.V. Leonidov, and P.V. Ruuskanen, Nucl. Phys. **B481**, 704 (1996).
[62] V.N. Gribov and L.N. Lipatov, Yad. Fiz. **15**, 781 (1972) [Sov. J. Nucl. Phys. **15**, 438 (1972)]; G. Altarelli and G. Parisi, Nucl. Phys. **B126**, 298 (1977); Y.L. Dokshitzer (in Russian), Zh. Eksp. Teor. Fiz. **73**, 1216 (1977) [Sov. Phys. JETP **46**, 641 (1977)].
[63] J. Bartels and E. Levin, Nucl. Phys. **B387**, 617 (1992).
[64] A.H. Mueller and D.N. Triantafyllopoulos, Nucl. Phys. **B640**, 331 (2002).
[65] A.H. Mueller, Nucl. Phys. **A724**, 223 (2003).
[66] V.A. Abramovsky, V.N. Gribov, and O.V. Kancheli, Yad. Fiz. **18**, 595 (1973) [Sov. J. Nucl. Phys. **18**, 308 (1974)].
[67] K. Golec-Biernat and M. Wusthoff, Phys. Rev. D **59**, 014017 (1999); **60**, 114023 (1999).
[68] D. Kharzeev, E. Levin, and M. Nardi, hep-ph/0212316.
[69] R. Baier, A. Kovner, and U.A. Wiedemann, Phys. Rev. D **68**, 054009 (2003).
[70] J. Jalilian-Marian, Y. Nara, and R. Venugopalan, nucl-th/0307022.
[71] J.L. Albacete, N. Armesto, A. Kovner, C.A. Salgado, and U.A. Wiedemann, hep-ph/0307179.